Institutionen för systemteknik
Department of Electrical Engineering

Examensarbete

Modelling of Cranking Behaviour in Heavy Duty Truck Engines

Examensarbete utfört i Fordonssystem
vid Tekniska högskolan vid Linköpings universitet
av

Erik Andersson

LiTH-ISY-EX--15/4822--SE

Linköping 2014

LINKÖPINGS UNIVERSITET

Linköpings universitet
TEKNISKA HÖGSKOLAN

Department of Electrical Engineering
Linköpings universitet
SE-581 83 Linköping, Sweden

Linköpings tekniska högskola
Linköpings universitet
581 83 Linköping

Modelling of Cranking Behaviour in Heavy Duty Truck Engines

Examensarbete utfört i Fordonssystem
vid Tekniska högskolan vid Linköpings universitet
av

Erik Andersson

LiTH-ISY-EX--15/4822--SE

Handledare: **Christofer Sundström**
ISY, Linköpings universitet

Examinator: **Erik Frisk**
ISY, Linköpings universitet

Linköping, 12 december 2014

Avdelning, Institution
Division, Department

Vehicular Systems
Department of Electrical Engineering
SE-581 83 Linköping

Datum
Date

2014-12-12

Språk
Language

☐ Svenska/Swedish
☒ Engelska/English
☐ ________________

Rapporttyp
Report category

☐ Licentiatavhandling
☒ Examensarbete
☐ C-uppsats
☐ D-uppsats
☐ Övrig rapport
☐ ________________

ISBN
—

ISRN
LiTH-ISY-EX--15/4822--SE

Serietitel och serienummer
Title of series, numbering

ISSN
—

URL för elektronisk version

`http://urn.kb.se/resolve?urn=urn:nbn:se:liu:diva-121289`

Titel
Title
Modelling of Cranking Behaviour in Heavy Duty Truck Engines

Författare
Author
Erik Andersson

Sammanfattning
Abstract

In modern heavy duty trucks the battery is a central component. Its traditional role as an energy source for engine cranking has been extended to include powering a number of electrical components on the truck, both during driving and during standstill. As a consequence of this it is important to know how much a battery in use has aged and lost in terms of capacity and power output. The difficulty in measuring these factors on a battery in use causes problem, since heavy duty truck batteries are often replaced too early or too late, leading to unnecessary high replacement costs or truck standstill respectively.

The overall goal of the effort, of which this thesis is a part, is to use a model of the cranking behaviour of a heavy duty truck engine, which depends on the battery condition, to estimate the ageing and wear of a heavy duty truck battery. This thesis proposes a modelling approach to model the components involved in engine cranking.

In the thesis work, system identification is made of the systems forming part of the cranking of a heavy duty truck engine. These components are the starter battery, the starter motor and its electrical circuit and the internal combustion engine. Measurement data has been provided by Scania AB for the evaluation of the models. The data has been collected from crankings of a heavy duty diesel engine at different temperatures and battery charge levels. For every cranking lapse the battery voltage and current have been measured as well as the engine rotational speed.

A starter battery model is developed and evaluated. The resulting battery model is then incorporated into two different engine cranking models, Model 1 and Model 2, including a starter motor model and an internal combustion engine model apart form the battery model. The two cranking models differ in several aspects and their differences and resulting evaluations are discussed.

The battery model is concluded to be sufficiently accurate during model verification, however the two cranking models are not. Model 2 is verified as more correct in in its output than Model 1, but neither is sufficiently accurate for their purpose. The conclusion is drawn that the modelling approach is sound but development of Model 2 is needed before the model can be used in model-based condition estimation.

Nyckelord
Keywords
Modelling, Cranking, Heavy Duty Diesel Engine, Battery Condition, Model Evaluation, Prediction Error Minimisation

Abstract

In modern heavy duty trucks the battery is a central component. Its traditional role as an energy source for engine cranking has been extended to include powering a number of electrical components on the truck, both during driving and during standstill. As a consequence of this it is important to know how much a battery in use has aged and lost in terms of capacity and power output. The difficulty in measuring these factors on a battery in use causes problem, since heavy duty truck batteries are often replaced too early or too late, leading to unnecessary high replacement costs or truck standstill respectively.

The overall goal of the effort, of which this thesis is a part, is to use a model of the cranking behaviour of a heavy duty truck engine, which depends on the battery condition, to estimate the ageing and wear of a heavy duty truck battery. This thesis proposes a modelling approach to model the components involved in engine cranking.

In the thesis work, system identification is made of the systems forming part of the cranking of a heavy duty truck engine. These components are the starter battery, the starter motor and its electrical circuit and the internal combustion engine. Measurement data has been provided by Scania AB for the evaluation of the models. The data has been collected from crankings of a heavy duty diesel engine at different temperatures and battery charge levels. For every cranking lapse the battery voltage and current have been measured as well as the engine rotational speed.

A starter battery model is developed and evaluated. The resulting battery model is then incorporated into two different engine cranking models, Model 1 and Model 2, including a starter motor model and an internal combustion engine model apart form the battery model. The two cranking models differ in several aspects and their differences and resulting evaluations are discussed.

The battery model is concluded to be sufficiently accurate during model verification, however the two cranking models are not. Model 2 is verified as more correct in in its output than Model 1, but neither is sufficiently accurate for their purpose. The conclusion is drawn that the modelling approach is sound but development of Model 2 is needed before the model can be used in model-based condition estimation.

Acknowledgments

I would like to thank my supervisor at LiU, Dr. Christopher Sundström, for his help and support during this thesis. I would also like to thank my examiner, Associate Professor Erik Frisk, for making the thesis and its results possible. For feedback and input I would like to thank Associate Professor Mattias Krysander and the group involved in battery studies at ISY.

A special thanks to my near and dear, Ingrid, Hans, Joel, Magnus, Helena, Filip, Alice, Elsa, Stefan, Astrid and Johan for their faith in me and their support for my work. Amongst the people to thank are also the student orchestra LiTHe Blås, Comdr. Shepard and mr Madden for providing valuable distractions to make the work easier.

Finally I thank you, Alexandra, for your help when things are tough, your toughness when work is hard and your joy when things are easy. I love you.

Linköping, January 2015
Erik Andersson

Contents

1 Introduction **1**
- 1.1 Objectives . . . 2
- 1.2 Outline and Contributions . . . 2

2 Modelled System and Physical Background **5**
- 2.1 Starter Battery . . . 5
  - 2.1.1 Chemical Reaction . . . 7
  - 2.1.2 Battery Model Structure . . . 7
- 2.2 Starter motor . . . 10
- 2.3 Internal Combustion Engine . . . 11
  - 2.3.1 Friction in Diesel Engines . . . 12
  - 2.3.2 Engine Pressure . . . 14
  - 2.3.3 Reciprocation of engine parts . . . 14
- 2.4 Data from Scania . . . 14

3 Models **17**
- 3.1 Battery Model . . . 18
  - 3.1.1 Dynamic Battery Parameters . . . 19
- 3.2 Starter Motor Model . . . 23
  - 3.2.1 Used Variations of the Starter Motor Model . . . 25
- 3.3 ICE Model . . . 26
  - 3.3.1 Engine Pressure Model . . . 26
  - 3.3.2 Reciprocating Elements . . . 28
  - 3.3.3 Friction Losses . . . 28
  - 3.3.4 Comment On the Friction Model . . . 31
  - 3.3.5 Summing Up the ICE Model . . . 32
- 3.4 Model Summary . . . 32

4 Parameter Estimation and Model Evaluation **35**
- 4.1 Grey-Box Estimation Using Data . . . 35
- 4.2 Battery Model Parameter Evaluation . . . 37
  - 4.2.1 Estimation . . . 37
  - 4.2.2 Verification . . . 41

4.3 Cranking Model Parameter Evaluation 45
    4.3.1 Estimation 45
    4.3.2 Verification 55

5 Conclusions 61
5.1 Future Work 62

Bibliography 63

1

Introduction

In modern heavy duty trucks the importance of the starter battery has increased. The electric source is no longer used only for cranking the engine, but also for maintaining power to a number of electrical components featured on modern trucks. In the last 15 years Scania trucks have gone from featuring 5 computing units to more than 20 per truck. In this context the condition, ageing and capacity loss of a truck's starter battery is relevant to the function of a high number of systems featured on a truck. Battery lifetime in vehicles of this type varies significantly and the underlying reasons are complex.

Normally a truck in active use does not have sensors monitoring the well-being of the starter battery for a number of reasons, one being that to accurately measure factors like the open circuit voltage and the internal resistance of a battery, it is needed to wait several hours after use of the battery for transients to fade out.

Cranking behaviour of a truck depends on a number of factors including ambient temperature, electrolyte temperature of the battery, temperature of the oil in the combustion engine and the general condition of the battery. Measurements needed for battery surveillance are normally not available for use in on-board diagnostics of heavy duty trucks. Therefore, the idea is to use available signals such as engine rotational speed and oil temperature together with a model for cranking behaviour in order to estimate wear, State of Charge and State of Health of a truck battery.

The thesis is a part of a project dedicated to investigating wear and lifetimes of heavy duty trucks and using statistical analysis, prognostics and modelling to do so. The project, IRIS, is a collaboration between the Institution for Electrical Engineering (ISY) at Linköping University, Scania AB and Stockholm University.

1.1 Objectives

The aim of the thesis is to investigate a model-based approach to measuring the condition of a heavy duty truck starter battery. The final goal of the project is to use a model of the cranking behaviour of a heavy duty truck to correctly asses the condition of a truck battery using measurements collected during cranking of the engine.

The goal for this thesis is to construct the model of the cranking of a heavy duty engine. The model is to be implemented in *MATLAB/Simulink*. For the purpose of calibrating the model, data has been provided, consisting of measurements of a cranking system used at different temperatures and varying battery charge levels.

The objectives of the thesis are:

- Investigate the system involved in cranking a heavy duty truck engine
- Investigate the structure and submodels needed to form a model of such a system
- Outline a physical state-space model of the system
- Implement the model in a manner that allows it to be fitted to the measured data
- Fit model to data
- Evaluate the ability of the model to duplicate measured signals
- Draw a conclusion on the viability of this modelling approach for the purpose of model-based condition estimation of heavy duty truck batteries

1.2 Outline and Contributions

Chapter 2 is a theory chapter containing general modelling principles applied in the thesis work as well as theory of the systems modelled. It also contains some modelling theory and sets the framework for the models used in the project.

The models developed during the work are presented in Chapter 3. The derivation of the models and their sub-models are explained and their states and parameters are listed. The work on this chapter includes system identification of the cranking system and its significant components.

The model structure presented in Chapter 3 has been evaluated to fit the models to data. The model evaluation progress is presented in Chapter 4 which includes both fitting of the models to data and verification of the model accuracy. The chapter demonstrates how well the models can be fitted to data and the methods used during the model evaluation.

Chapter 5 contains the conclusions of the thesis and possible directions for future work on the project.

The contributions by the author of this thesis are presented in Chapters 3, 4 and 5. The models introduced have got a physical foundation and are designed by the author. In the cases where a model is based on a model in literature the earlier model is stated and its originator credited. The software for model parameter estimation and model simulation has been developed, in *MATLAB/Simulink*, by the author. The conclusions of the thesis stem from the author and the work done on the thesis.

2

Modelled System and Physical Background

This chapter contains a theoretical background to the systems that have been modelled throughout the thesis project, as well as modelling basics and principles. The system that needs modelling to correctly represent a cranking procedure includes three major components, the starter battery, the electric starter motor and the internal combustion engine. The battery provides the electric power to drive the electric motor. The electric motor is then connected to the crankshaft of the engine and drives the crankshaft in order to build up pressure, airflow and temperature sufficient for ignition. The layout of this system can be seen in Figure 2.1. These three components together with external conditions like ambient temperature affect the cranking behaviour. The aim of this chapter is to give a good enough understanding of the components to proceed with the modelling concerned in the thesis. Aspects of the subjects that are not relevant for the modelling work is left out.

2.1 Starter Battery

The battery type most commonly used in cranking applications of vehicles is the Lead-Acid accumulator. The basic structure of this rechargeable battery dates back to the mid-19th century. It is the earliest form of rechargeable battery invented. The battery consists of two electrodes (metal plates) immersed in electrolyte. During charge or discharge one electrode functions as anode and the other as cathode. The electrode that serves as anode during discharging forms the negative pole of the battery and is made from lead (Pb). The other electrode (cathode when discharging) therefore is the positive pole and it consists of lead dioxide (PbO_2). This setup is illustrated in Figure 2.2.

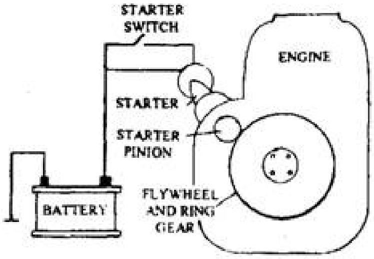
STARTER
SWITCH
ENGINE
STARTER
STARTER
PINION
BATTERY
FLYWHEEL
AND RING
GEAR

Figure 2.1: *The system involved in cranking an engine: starter battery, starter motor and the ICE [1].*

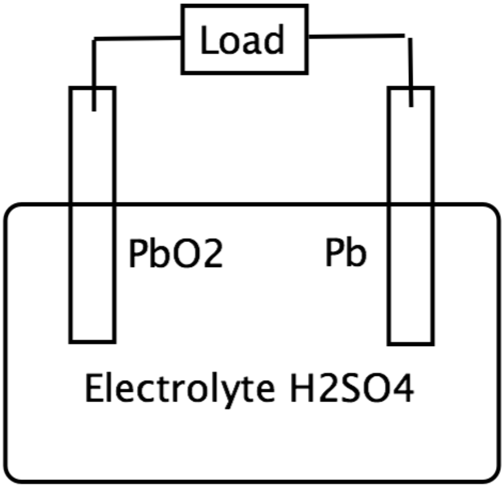
Load
PbO2
Pb
Electrolyte H2SO4

Figure 2.2: *Illustration of the electrochemical set-up of a lead-acid battery.*

2.1.1 Chemical Reaction

The chemical reactions taking place at each plate during discharge are the following. At the negative plate (anode during discharge):

$$Pb + HSO_4^- - 2e^- \rightarrow PbSO_4 + H^+ \tag{2.1}$$

At the positive plate (cathode during discharge):

$$PbO_2 + HSO_4^- + 3H^+ + 2e^- \rightarrow PbSO_4 + 2H_2O \tag{2.2}$$

During charging an external DC power source is applied instead of the electric load, forcing the current the other way, reversing the reaction.

For a car lead-acid battery it is normal to use six battery cells in series, each with a maximum voltage output of 2,1 V at full charge, producing a maximum battery voltage of 12,6 V. The type of heavy duty trucks treated in this thesis normally use two of these batteries in series to produce a 24 V system for starting the engine and running electrical components on-board. In reality batteries of this type can reach up to 25,2 V when the battery is fully charged. During charge even higher voltage is imposed over the battery's poles to provide enough potential difference to reverse the chemical reaction.

An introduction to the chemistry, design and implementations of lead-acid batteries is given in [17]. For vehicular batteries and their use, see [14], [28] and [13].

2.1.2 Battery Model Structure

Various model structures may be used when representing the characteristics of a physical battery. A detailed description of lead-acid batteries is given, in Chapter 16 [17], with origin in the chemical reaction briefly described above. An electrochemical model would be an alternative in modelling the characteristics of this type of battery. Such a model is centred around the reactions at the electrodes. Using states for the active matter at any time instant it is possible to calculate the power output of a battery. However, this comes at a high cost of model complexity. Some useful properties such as internal resistance are difficult to obtain from electrochemical reactions in the battery. There are also electrochemical factors in a battery that are not relevant to the external circuit, for example the amount of reactive mass in the battery. An electrochemical model is too detailed for the purpose of this thesis [13].

A second approach to modelling that is common in physical studies of a battery is the numerical modelling approach. It is very useful when studying physical systems that include a complex geometry. To calculate thermal transfer or mechanical stress in these systems a numerical solution using the Finite Element Method (FEM) is commonly used. The approach in this method is to divide the structure into a high number of small elements and subsequently solve the dynamic governing equations for the system numerically. This involves solving a number of non-linear equations iteratively putting a high demand on computation capacity [25] [13].

One more commonly used method is the equivalent circuit method. It involves approximating the characteristics of a complex electrical system in a smaller one. An example of a simple equivalent circuit of a battery using static (constant) parameters can be seen in Figure 2.3. This equivalent circuit incorporates an ideal voltage source, E_m, with a constant internal resistance, R, to generate the terminal battery voltage, U_b. This forms an idealized model of a battery as a voltage source with an inner battery resistance. If used with constant model parameters this model delivers a constant output voltage and, if connected to a load, a current. With constant parameters any change made on battery input would generate a instantaneous change in battery output. Were the parameters to be made dynamic it could model voltage drop as a function of the battery exhaustion or limitations given by external temperature variation. Non-linear dynamic parameters may be used in this linear battery model. The model, however, would not be able to model the fast dynamic behaviour of a real battery circuit.

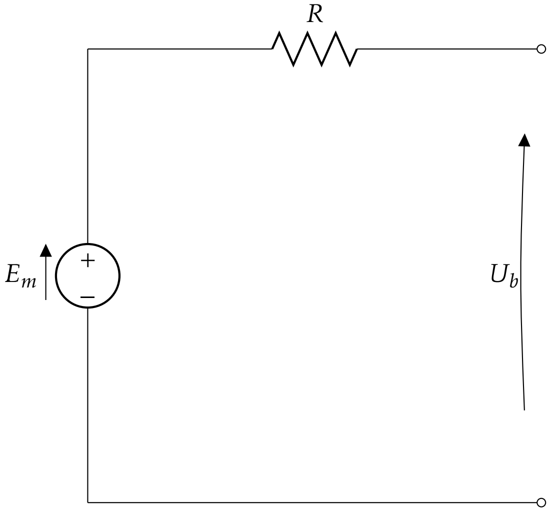

Figure 2.3: *Static equivalent circuit model of a battery.*

By adding elements to the circuit like capacitors and several resistances more dynamics can be modelled. In [13] and [28] the Randle equivalent circuit is considered. A Randle circuit is a type of Thevenin equivalent circuit that can use RC-elements in order to model otherwise complex dynamic behaviours when designing an equivalent circuit. With static (constant) parameters these types of circuits can represent the dynamic voltage output behaviour of a battery but not a number of other aspects such as representation of voltage drop as a result of extracted current over time. A voltage drop as result of current drawn from the battery is modelled by Ohm's law as a current passes through the internal resistance. However, as current is drawn from a battery over time the internal reactive substance depletes and the battery drains. To model this dynamic parameters are needed. Also the capacity of a real battery is limited and to get a detailed enough model one needs to monitor the percentage of the battery's capacity remaining and include a function for the voltage drop as a result of this state. The type of equivalent circuit demonstrated in [28] is illustrated in Figure 2.4. It consists of the basic electromotive force (Em), the internal resistance of the battery (R0), a capacitance (C1) and what is called an over-voltage resistance (R1). The output of the model is the terminal voltage U_b. In [8] the over-voltage resistance is said to represent the non-linear resistance resulting from the contact between the plate and the electrolyte in the battery.

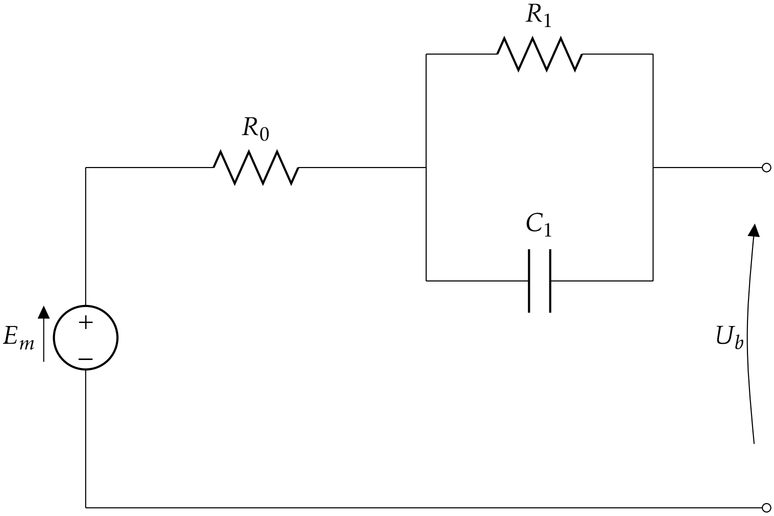

Figure 2.4: *Thevenin battery model.*

This model is referred to as the Thevenin Battery Model and is occasionally used for the type of modelling used in this thesis [6], [8]. In these cases all parameters are assumed to be constant which is problematic since the real values of these depend on battery conditions.

Regardless of which type of battery model that is used, there will be a need to represent the battery behaviour by model equations using parameters and state variables to represent the battery output from a given input. In Chapter 4 of [14] an introduction to two different battery modelling approaches is presented, quasistatic and dynamic modelling. They differ in what variables are used as inputs to the model and their modelling equations (though the same in both models) are used differently. For the quasistatic model the terminal battery power is used as input and the battery charge is considered as an output. In this case the battery discharge current and the battery voltage are considered as internal variables of the model. For a dynamic battery model the extracted current is used as input while the battery's terminal voltage is used as output.

More complex equivalent circuits are also used in research and design of battery-related systems, but the choice of battery model for this thesis will be discussed in Chapter 3.

2.2 Starter motor

An illustration of the principles of producing mechanical rotational energy using a Direct Current (DC) motor is presented in Figure 2.5. The current supplied from a lead-acid battery will be DC, thus DC-driven motors are used for cranking vehicles.

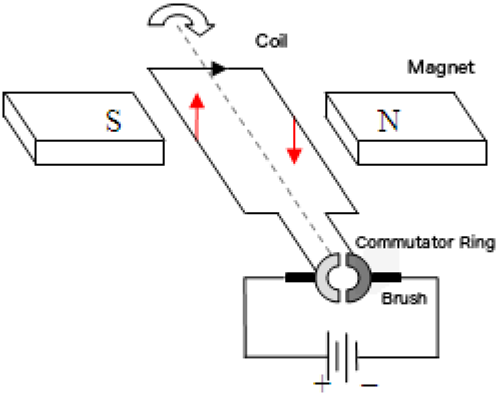

Figure 2.5: *Illustration of the principle of a DC motor [2].*

The principle of the DC motor as illustrated in Figure 2.5 can summarily be described as follows. Current from an external source is transferred via the brushes to the commutator ring and through the coil of the motor. The coil is a part of the rotating part of the motor, the rotor, which is why current is transferred via brushes in contact with the static part of the motor. The magnetic field then results in a magnetic force on the coil that can be illustrated by the right hand rule for an electric conductor in a magnetic field. For this to occur the external magnetic field and the coil need to be aligned as the picture demonstrates. When the directions are as in Figure 2.5 the magnetic forces resulting from the coil interacting with the external magnetic field result in a turning of the rotor generating mechanical rotational energy [12] [5].

As can be seen in Figure 2.5 the commutator ring connecting the brushes to the coil has two gaps in them. When the commutator rotates and the brushes reach this gap there is no current and therefore no magnetic force. At this point rotation continues because of inertia in the rotor. Once the brushes have past the gap in the commutator ring the direction of the current is back to the orientation of Figure 2.5 and the process repeats itself. The external magnetic field can be generated either by permanent magnets or coils generating an electromagnetic field. In the later case these coils would also need to be supplied with current from an external source. If the external magnetic field is generated by electromagnets we say that the stationary component (stator) is wounded, i.e composed of coils [12] [5] [14].

Brushed DC motors are constructed with wound rotors and either wound or permanent-magnet stators. The type used in engine cranking uses wound stators. There are several possible configurations in wiring the motor. The armature windings and the field coil can be electrically connected either in series or in parallel. There also exists a version named compound configuration that does both. The connection of the electrical components is illustrated in Figure 2.6. An overview of electric starter motor configurations can be found in [14]. The choice to be made is to either connect the coil winding and the field (stator) winding in series or parallel. A third alternative named shunt is a combination of the two. Normally in cranking the series wound configuration is used since this offers the best torque characteristics for the considered application. The delivered torque is proportional to the square of the current through the circuit, $T_{em} \propto I_{em}^2$. This yields a higher maximum torque at high loads which is suitable for cranking [12].

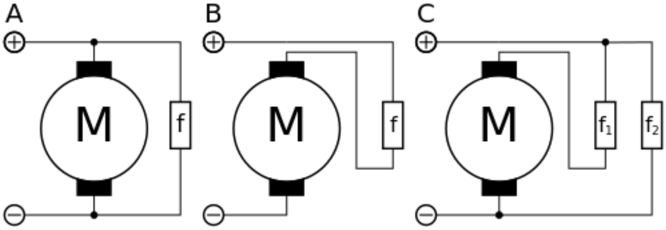

*Figure 2.6: Different winding connections of DC motors [15].
A: Shunt (parallel) B: Series C: Compound*

2.3 Internal Combustion Engine

The third element of the cranking model shown in Figure 2.1 is the internal combustion engine (ICE). All of Scania's heavy duty trucks use four-stroke diesel engines so this thesis will be limited to these [4]. A good general picture of diesel and other combustion engines is given in [11]. Diesel engines are compression-ignited engines (CIEs) that use the heat and pressure of compression in order to ignite the diesel air mixture in the cylinder.

Since the aim of the thesis is to model the cranking behaviour of an engine, the properties of the engine before the first ignition of an engine start are the relevant ones. The data sets provided by Scania are limited to cold starting of engines and so will the model be. There are a number of factors that influence the engines resistance to cranking. Essentially the model needed for this project needs to act as a resistance since the energy delivered by a combustion engine depends on the combustion of the fuel and during cranking there is no ignition. Assumptions, simplifications and delimitations of the modelling process will be discussed in Chapter 3 when the models used are specified.

When cranked during cold start an ICE resists motion in a number of ways. Since there is no ignition the engine produces no torque of its own. The sources for the engine's resistance are as follows:

- Friction
- Compression work
- Reciprocation of engine parts

2.3.1 Friction in Diesel Engines

Friction in a four-stroke engine originates in the contact surfaces between the moving parts (piston rings, bearings etc) and the fixed engine parts (cylinder lining, engine block etc). Each surface of contact and friction yields a component of the total friction in the engine. When modelling friciton in a combustion engine there are a few approaches available. The earlier mentioned book, [11], focuses on mean-value engine modelling. Mean-value engine modelling means that all variables such as inlet manifold pressure, combustion energy and engine friction are averaged out over each cycle. This makes the models less complicated and improves runtime but means that there is no insight on the in-cycle variations. This is very useful when modelling an engine that is running. Conditions for cold-starting of an engine are very different from those of an engine that has been running for some time as mentioned in [11] and [29]. Thus it is more probable that an instantaneous friction model will be used to provide a value of friction components at every instant during cranking.

The ICE model components in Section 3.3 are defined to give the engine pressure and reciprocating torque losses at any instant or crankshaft angle, θ, thus giving their contributions on instantaneous form. In [26] an attempt is made at determining the instantaneous friction torque in ICEs by using engine speed, $\dot{\theta} = \omega$, and indicated pressure, p_{cyl}. However, this model does not, account for the effect of temperature on the friction of the engine and does therefore not include any temperature dependence in the resistance of the engine. The instantaneous model in [27] scales the friction according to the Stribeck Curve that is exemplified in Figure 2.7. Thus Sandoval defines the friction losses as a polynomial function of engine speed with one constant, one linearly dependent on engine speed and one dependent on the square of the engine speed. This study mentions the effects of the temperature on the oil viscosity but demonstrates the friction loss effects over only a range of various engine running speeds. Thus, no insight is given on the friction behaviour during cold starting.

Another study that in great detail describes the instantaneous friction torque in a diesel engine is [7]. This describes the fluctuations of the different torque components over the entire engine cycle. In [7] the sources of mechanical friction in the ICE are given as piston rings, piston skirt, valve train, auxiliaries and bearings which concurs with [26] and [27]. However, [7] also classifies the different friction components over a range of operating points of the engine, varying over engine speed and load. The lowest engine speed considered is 1000 rpm, meaning that the effect of friction in cold starting is left out.

In an ICE all friction takes place under lubrication. One of the basic differences between a two-stroke and a four-stroke vehicle engine is the way of lubricating the engine. In a two-stroke the motor oil is mixed with the fuel to provide lubrication of the moving parts. In a four-stroke the motor oil is kept separate from the fuel and the moving parts are supplied with oil from a capacity pan at the base of the engine and an oil pump is used to transport oil into bearings and joints. This is called a wet sump lubrication system. The oil then drains into the pan due to gravitation. Thus, the temperature in the cylinder and oil temperature are only indirectly linked through heat transfer in the engine block. This all serves to make sure there is an oil film between all moving parts and their adjacent non-moving parts.

The characteristics of the friction between the metal parts of an ICE are determined by the mode of lubrication between the two. Depending on the thickness of the oil film the friction coefficient varies in different ways. The domains of this variation can be described in a Stribeck diagram. These diagrams are mentioned in [7] and [29]. A simplified version is given in [9] that gives an approximation of the mixed and hydrodynamic domains of the friction. Essentially the domain that gives the behaviour of the friction dynamics is determined by the thickness of the oil film, viscosity of the oil and the speed of motion. The speed of motion in this case can be represented by the orthogonal speed of the piston. An illustration of the Streibeck curve for different domains of lubricated friction is shown in Figure 2.7.

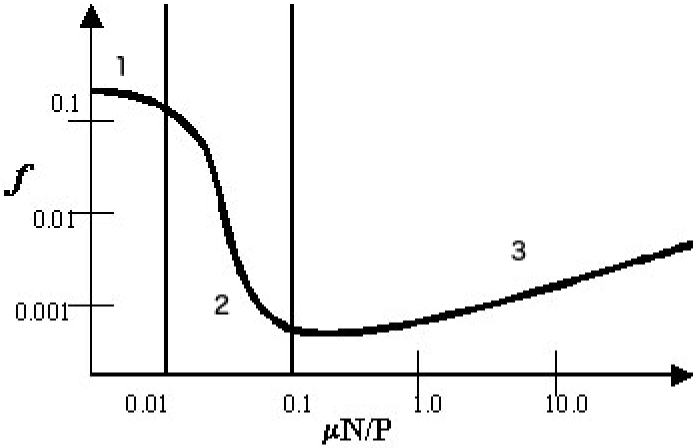

Figure 2.7: Stribeck Curve to illustrate different domains of friction [3].
1: Solid/Boundary friction
2: Mixed Friction
3: Hydrodynamic/Fluid Friction
On the Y-axis in the picture is the friction coeffitent and on the X-axis is the load parameter that governs the friction domain, $\mu N/P$. This load parameter consists of oil viscosity, μ, speed of motion, N, and load on the surface, P, i.e oil film thickness.

In a well-lubricated engine most friction between surfaces work under hydrodynamic friction condition. Some exceptions can occur, however. For example when the piston is around the top dead centre (TDC) the oil film around the edges breaks down and is thinned out, leading to a change in domain from hydrodynamic friction to the mixed domain [29]. As illustrated in Figure 2.7 this yields different characteristics in friction as the duty parameter varies. The essential difference between the two situations is that the oil film is thinner closer to TDC. The boundary domain is caused by an even thinner oil film between components. Friction at this point is close to dry friction (metal on metal in a truck engine) and needs to be avoided since it might cause an engine to break down completely. In a normal running case this type of friction does not occur in an ICE.

2.3.2 Engine Pressure

As mentioned in the introductory part of Section 2.3 this thesis aims to model the cranking of the engine. The diesel engine is electrically cranked to provoke ignition at which point combustion drives the engine instead of the external cranking system. Diesel engines are Compression Ignited Engines (CIEs). Thus the engine must build up a pressure and temperature sufficient enough to ignite the fuel-air mixture when cranking. Since no combustion takes place during this cranking the only indicated pressure in the cylinder stems from the air-fuel mixture being compressed by the cylinder.

The compression work is the work used to compress the air-fuel mixture in the cylinders during cranking. It is determined by the pressure in the cylinders, the dimensions of the combustion chamber and the lever between the chamber and the crankshaft. When air is compressed in the cylinder work is used to do the compression. After the piston has passed TDC it in turn delivers torque to the crankshaft since the expansion of air-fuel mixture then provides a force on the piston head that aids the cranking for the duration of the expansion [11].

During compression in an ICE all valves in the cylinder are closed meaning that the air compression is a function of the size of the combustion chamber given by the position of the piston and the pressure in the cylinder when the compression begins. It is normal for diesel engines to generate a pressure of about 40 bar (4,0 MPa) and a temperature in the cylinder of about 550 °C for ignition to take place [11].

2.3.3 Reciprocation of engine parts

The loss due to reciprocation of engine elements is the resistance to movement by the parts that are accelerated during engine rotation. Force caused by acceleration of a mass is given by Newton's second law, $F = ma$. This will occur during vertical, lateral and rotational acceleration in the engine.

2.4 Data from Scania

This section provides an overview of the available data. For more details on the use of the data in model evaluation, see Section 4.1. The data is in time-domain form which means that all data is provided as measured data over time. The data has been collected in a controlled-environment engine test cell at Scania. It consists of measurements of selected variables during cold start cranking of heavy duty engines. Three heavy duty diesel engines have been used for the data collection with five, six and eight cylinders. This thesis will focus on the cranking modelling of one of the engines since the principles are the same for all engines and a completed model can be extended and validated for another engine. Thus the meaning of "model evaluation data" for the remainder of this thesis will be the measured data for a five cylinder diesel engine, the Scania DL5.

The measured data from cold start cranking of the Scania DL5 consists of time series data of a number of engine quantities. An engine has been cranked until ignition occurs at controlled temperatures of +35°C, +10°C, 0°C, -10°C, -15°C, -20°C and -25°C. At every temperature the starter battery powering the cranking has been fully charged before the first cranking attempt and then a number of cold starts at each temperature have been made until the battery is no longer able to crank the engine enough to achieve ignition. In some cases several of these battery discharge lapses have been made with a fully charged battery at the beginning of each test. For the majority of the cold starts data has been collected with a measurement frequency of 5000 Hz with the exception of 8 starts at +10°C where the measurement frequency is 5 Hz. The data includes measurements of:

- Fuel pressure
- Battery current
- Battery voltage
- Engine rotational speed

A plot of measured engine rotational speed and current drawn from the battery during a measurement series at 0°C can be seen in Figure 2.8.

When the data has been collected the engine has been given time to cool between each cranking to ensure cold starting conditions. In the cases where the engine is able to ignite and start running the engine has been cut just after ignition in order to minimize cool down time between starts. In each case measurements begin just before each cranking and end just after in order not to miss any details. This means that the data contains extra information not relevant to the cranking. Therefore the relevant data has been isolated from the unnecessary data by isolating the part of each series that contains the data for the cranking and isolating the desired variables during this time window. The use of this data in setting parameters for the models is described in Section 4.1.

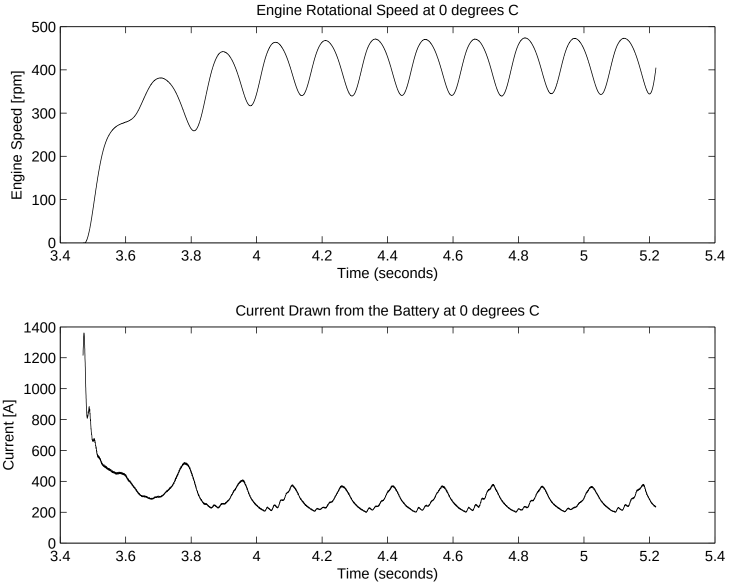

Figure 2.8: *A plot of two typical measured signals, engine rotational speed and battery current collected during a cranking at 0°C.*

3

Models

This chapter treats the models used when modelling the cranking behaviour of the truck engines. It contains the postulations and simplifications that have been made in the modelling process as well as the modelling equations and an overview of the final model.

The basic configuration of the system involved in cranking a heavy duty truck ICE is explained in Chapter 2. An overview of the system and its causality can be seen in Figure 3.1.

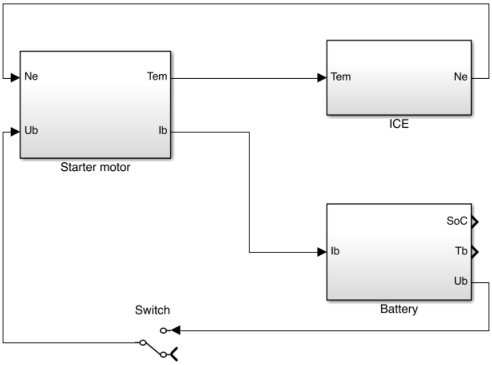

Figure 3.1: *Model structure of the cranking system of a diesel engine.*

For the three submodels in Figure 3.1 there are signals forming their respective interface. The battery voltage output, U_b, provides an electromotive force for the starter motor circuit. Through the windings in the armature of the motor the starter motor model generates the torque, T_{em}, used for cranking the ICE. The current consumed in the circuit is considered as an input to the battery model. Thus the battery model can represent the battery draining as current is drawn from it. The electric motor is mechanically connected to the crankshaft of the ICE and thus the electric machine torque T_{em} turns the engine during cranking. The rotational speed of the ICE, ω, is fed back to the starter motor model to model the back EMF.

A large portion of the model parameters of the ICE model stem from the friction model. As to the complexity level of the friction model used, the foundation is in [29], which in turn is an improvement on the model developed in [26]. The complexity increases as more and more detailed processes are included in the model. It is however evident when the model from [29] is improved in [7] that such complexity is needed to accurately model engine friction in an instantaneous manner. Another approach is taken in [27] with mean-value friction models for a similar engine. The mean-value models differ in their structure, but their model equations are equally complex and non-linear to the ones presented in [29]. When a simplified friction model is developed in [18] the friction model becomes more simple at the price of a higher number of states used in the friction model.

In the modelling of this thesis two models have been introduced. For the remainder of the report they will be referred to as Model 1 and Model 2. They both follow the same basic structure, differing a bit in number of model states and parameters used. They both use the same battery model, their differences stem from varying applications of the starter motor and friction models. Their differences will be explained in Sections 3.2.1 and 3.3.4, and the states and parameters of each model will be summed up in Section 3.4. The models represent two different generations of the complete model of this thesis, Model 1 being the earlier one. The aim is that Model 2 will therefore prove better in some aspects than Model 1. They are also both included because their differences make them interesting to compare when drawing conclusions on the model evaluation in the thesis.

3.1 Battery Model

A general introduction to lead-acid accumulators is presented in Section 2.1. In [14] two general causality approaches for battery modelling are presented, quasi-static modelling and dynamic modelling [20]. Simply put they differ in what variables are defined as inputs and outputs of the battery model (their causality) and in accordance the different approaches use their modelling equations differently. The dynamic models are usually able to describe the transient behaviour of batteries, including the rate of change of the battery terminal voltage [14]. It also gives physical insight and fits well with the causality idea presented in Figure 3.1.

As is mentioned in Section 2.1 various approaches can be taken when modelling a battery. In this thesis the choice has been made to apply an equivalent-circuit model with dynamic parameters. The dynamics of a battery delivering voltage can be obtained from this but it does not give any insight as to the internal chemistry or workings of the battery [17], [14]. An equivalent circuit that incorporates RC or RL elements with constant parameters can quite well approximate the dynamic in delivering electricity, but lacks the ability to describe the effects of discharging a battery over time such as increased internal resistance and drop in terminal voltage. Therefore the dynamic parameters are essential when using an equivalent circuit to describe battery discharging at different temperatures and levels of charge. An overview of various modelling approaches is presented in [28]. Here one can also see the manner in which a Randle circuit constructed of a series of RC parallel circuit elements can model dynamic behaviour using a number of parameters for the different RC elements. Souzzo demonstrates in [28] that a lot is gained in terms of representing dynamics behaviour simply by using a Randle model of order 1, incorporating one RC element in the circuit.

The version of this model that forms the basis for the battery model that is to be used is developed by Robert Jackey in [16], where a first degree Randle model is developed and complemented with a parasitic leak branch. Jackey also states expressions for dynamic parameters in the model, that are parametrized in [24] and [16]. The model used by Jackey is modified for the use of this thesis. In [16] Jackey states that the parasitic branch representing leak current in the battery is significant during charge at high SOC. In the data provided for this thesis there is no information on the charging of the truck batteries to be modelled and thus no need to model battery charging at high SOC. Thus the parasitic branch is left out, yielding the equivalent circuit structure presented in Figure 2.4. A model state will be needed for modelling the voltage drop across the RC element since this essentially works as a first-order time delay for the voltage.

The model structure in Figure 2.4 can model the dynamic voltage characteristics with reasonable accuracy while using three model states. This structure together with dynamic parameter equations presented in [16] forms the battery model chosen for this thesis. The model parameters will need to be set in order to accurately model the specific type of battery used in Scanias truck systems.

3.1.1 Dynamic Battery Parameters

All parameters of the battery model are demonstrated in the illustration of the model structure in Figure 2.4. Each electric component is designed to emulate a certain aspect. The dynamic equations are primarily designed to represent the behaviour of the battery as a function of discharge over time. The non-linear parameter equations are consisting of states and empirical parameters that need to be set according to the battery that is to be modelled.

Battery EMF

The electromotive force of the battery model is provided by the ideal voltage source E_m. As stated in among others [17] and [14] there is a maximum voltage for lead-acid accumulators of about 2 V. This is for good operating conditions and full battery charge. Both [17] and [13] state that output voltage of the battery declines with increasing temperature and decreasing State of Charge. This is here modelled by the following expression for the ideal voltage:

$$E_m = E_{m0} - K_E \nu_{bat}(1 - SOC) \tag{3.1}$$

Here E_{m0} is the ideal output voltage of a lead-acid accumulator, K_E is a model parameter constant, ν_{bat} is the battery electrolyte temperature in K and SOC is the battery State of Charge. ν_{bat} and SOC are functions of other battery variables and will be explained further on in this chapter. This gives a linear dependence between battery EMF and temperature, since the battery's ability to deliver voltage goes down with rising temperature [17] [16]. In (3.1) the battery EMF level decreases when the battery heats up. In the same manner E_m decreases as current is extracted from the battery, reducing the charge level.

Battery Capacity

The battery capacity model represents an approximation of the total battery capacity as a function of the current discharging from the battery and the battery temperature. As mentioned above the capacity as well as the output voltage of a battery varies with changing temperatures. Both these are lowered by high temperatures. Presented in (3.2) is a non-linear empirical equation that uses drawn current and battery temperature to model battery capacity. The temperature variation in capacity is given through a look-up table (LUT), $K_t(\nu_{bat})$. The expression for the capacity is given as:

$$C(I, \nu_{bat}) = \frac{K_c C_{0^*} K_t(\nu_{bat})}{1 + (K_c - 1)(I/I^*)^{\delta}} \tag{3.2}$$

The expression in (3.2) includes two model parameter constants, δ and K_c. Out of the two currents in (3.2) I^* is a nominal battery current and I is the current extracted from the battery. The constant C_{0^*} is the battery capacity with no external load at 0°C, and the unit of $C(I, \nu_{bat})$ is Ampere-seconds [16].

Extracted Battery Charge

The extracted charge of the battery is simply the integration of the current flowing out of the battery main branch. Thus the expression for extracted battery charge is:

$$Q_e(t) = Q_{e,init} + \int_0^t -I(\tau)\mathrm{d}\tau \tag{3.3}$$

Here $I(t)$ is the current extracted from the battery in Amperes, t is the simulation time of the model in seconds, τ is the integration variable and $Q_{e,init}$ is the charge that has been extracted from the battery prior to the start of simulation.

State of Charge and Depth of Charge

This battery model uses two different types of comparative measure of the charge level of the battery, State of Charge (SOC) and Depth of Charge (DOC). The difference between the two is that SOC is a measure of the remaining charge of the battery compared to the ideal maximum capacity of the battery while the DOC measures the remaining charge in the battery compared to the capacity at the current average main branch current, $I(t)$. For SOC the capacity is taken as when the battery is fully charged. Using the expression of the battery capacity introduced in (3.2), extracted charge from (3.3) and average current from (3.4) the expressions for SOC and DOC are given in (3.5) and (3.6). The average current used in the expression for DOC is calculated using (3.4). It is estimated using a first-degree averaging system. It averages the main branch current using a model parameter time constant, τ_1. The expressions for SOC and DOC used are defined in [16].

$$I_{avg} = \frac{I}{\tau_1 s + 1} \tag{3.4}$$

$$SOC = 1 - \frac{Q_e}{C(0, \nu_{bat})} \tag{3.5}$$

$$DOC = 1 - \frac{Q_e}{C(I_{avg}, \nu_{bat})} \tag{3.6}$$

Large discharge currents means that the battery drains quicker, and therefore DOC will always be less than or equal to SOC.

Terminal Output Resistance

The resistance over the battery terminals is considered an external resistance to the chemical battery reactions and therefore depending only on the state of charge and not the battery electrolyte temperature. The resistance R_0 is calculated as:

$$R_0 = R_{00}\left[1 + A_0(1 - SOC)\right] \tag{3.7}$$

In this expression R_{00} is the terminal resistance when the battery is fully charged. A_0 is a model parameter constant.

Battery Parallel Resistance

Battery parallel resistance is the resistance R_1 of the parallel RC element in the battery equivalent circuit. It is depending on DOC. When the battery discharges this exponentially influences the internal parallel resistance. Thus the expression becomes:

$$R_1 = -R_{10}\log(DOC) \tag{3.8}$$

In this expression R_{10} is a constant model parameter. The logarithmic expression represents an exponential increase of resistance as DOC decreases. However, since a battery will reach its terminal voltage where it is deemed discharged for cranking purposes well before the DOC reaches 0. The minimal SOC present in the data is around 0,2.

Battery Capacitance

A parallel RC element of a circuit basically translates into a time delay of the voltage. In modelling terms it equals a first-order system. In this circuit the capacitance of the capacitor gives the length of the time delay. Thus the expression is:

$$C_1 = \frac{\tau_1}{R_1} \tag{3.9}$$

In this expression τ_1 is a time constant of the model and its unit is seconds.

Battery Electrolyte Temperature

Since all currents in the battery passes some form of resistance they will generate heat in the battery causing the battery electrolyte to heat up during both charging and discharging. The thermal model uses a first order differential equation for the battery electrolyte temperature with parameters representing the battery's thermal resistance R_θ and thermal capacity C_θ. This yields:

$$\dot{\nu}_{bat}(t) = \frac{\left[P_s - \frac{\nu_{bat}-\nu_{amb}}{R_\theta}\right]}{C_\theta} \tag{3.10}$$

Here P_s is the power developed through $P = RI^2$ in R_0. Since the model is of cold starting engines the electrolyte temperature is initially assumed to be the same as the ambient temperature also used in the expression, ν_{amb}. The simulation time is taken as t and τ is the integration variable.

Comments on the Battery Model

In order to model six individual battery cells one would need to include another heat transfer model since the six cells are placed in a row in the battery and heat will be transferred through the battery [28]. This is not done in this thesis as the aim is primarily to accurately model the cranking behaviour.

The battery model uses five internal states to generate its output of terminal voltage. The states are electrolyte temperature (ν_{bat}), extracted battery charge (Q_e), average discharge current (I_{avg}), voltage drop over the parallel branch (V_c) and ambient temperature (ν_{amb}). The ambient temperature is considered a static state as we assume that the external temperature is not changed during cranking. The battery model has got five parameters that can be used to parametrize the model and adapt it to measured data. The parameters are the constant in the main voltage expression (K_E), the constant in the terminal resistance expression (Ao), the constant of the parallel resistance (R_{10}), the time constant in the capacitance (τ_1) and the second constant of the terminal resistance expression (R_{00}). The model uses one input, the current extracted from it, I.

3.2 Starter Motor Model

This section presents the model of the electric starter DC motor used in the cranking model. As mentioned in Section 2.2 the electric motor used for this type of cranking is series wound. This means that all components of the motor circuit are connected in series [12] [5]. The starter motor circuit is shown in Figure 3.2.

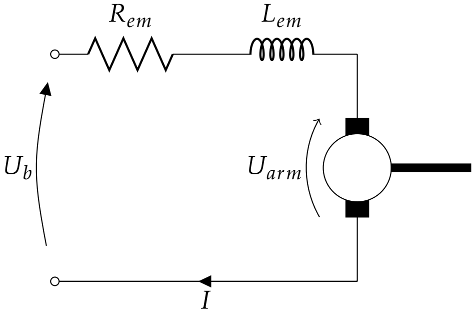

Figure 3.2: *Equivalent circuit of a series-wound DC motor.*

The voltage U_b is applied to the starter motor by the starter battery. The circuit consists of an inductance, L_{em}, in series with a resistance, R_{em}, and an armature that produces the torque of the motor. Once the voltage is applied to the circuit the current I flows through all components. When the motor starts rotating the armature voltage, U_{arm} becomes the back electromotive force. The back EMF is therefore the voltage that is induced into the circuit as a result of the motor's conductors moving in relation to the magnetic field in the armature [12] [14] [5]. When the circuit current drives a motor the back EMF works against the applied external voltage. If a circuit of this type is used as a generator the turning of the armature induces the voltage at the circuit poles. The back EMF is given by:

$$V_{arm} = K\Phi\omega_{em} \tag{3.11}$$

In (3.11) K is a motor constant, Φ is the magnetic flux in the armature and ω_m the angular velocity of the electric motor. The motor constant depends on design parameters of the motor [12], and the torque developed by the starter is:

$$T_{em} = K\Phi I \tag{3.12}$$

The magnetic flux is proportional to the magnetic field current, $\Phi \propto I_{field}$ [12]. Since the motor is series wound the current running through the armature is also the field current of the DC motor, meaning that the magnetic flux can be given by:

$$\Phi = K_F I_{field} = K_F I \tag{3.13}$$

In (3.13) K_F is a constant that depends on the number of field windings in the motor, geometry of the magnetic circuit and the magnetic characteristics of the iron in the armature. This constant can be affected by phenomena such as magnetic saturation when a magnetizing field fails to magnetize the iron further, causing a saturation behaviour. Since the DC motor can here be said to operate at a linear range, K_F is approximated with a constant [12].

Combining the expression for the flux with the EMF and torque equations yields:

$$V_{arm} = KK_F\omega_m I = \kappa_{em}\omega_m I \tag{3.14}$$

and

$$T_{em} = KK_F I^2 = \kappa_{em} I^2 \tag{3.15}$$

In (3.14) and (3.15) the earlier constants have been combined for model simplicity according to $\kappa_{em} = KK_F$. Together with the induction and resistance in the starter motor circuit the differential equation governing the starter motor current is given by:

$$\dot{I} = (U_b - R_{em}I - \kappa_{em}\omega_m I)/L_{em} \tag{3.16}$$

In (3.16) U_b represents the external voltage applied to the circuit. For this system U_b is the voltage supplied by the truck's starter battery. From a causality point of view the torque given by (3.15) and the current given by (3.16) are considered the outputs of the starter motor model, the current serving as input to the battery model and the generated torque propelling the cranking of the ICE. The inputs of the starter motor model are the battery voltage applied to the circuit and the rotational speed of the ICE crankshaft.

The starter motor armature to this point is considered an ideal electrical machine coupled with two electrical elements in the circuit [5]. It is possible to extend this model to also include a model of the inertia of the moving parts of the electric motor. In that case there is a mechanical time constant in the system based on the inertia of the starter motor, J_{em}. According to [22] the friction of a starter motor can also be well approximated with a constant. That leads to (3.17) which governs the rotational speed of the motor.

$$\dot{\omega}_{em} = \left(T_{em} - T_{fric,em} - T_{load}\right)/J_{em} \tag{3.17}$$

The components of (3.17) are the rotational speed of the starter motor (ω_{em}), the torque produced by the motor's armature (T_{em}), the constant friction of the motor ($T_{fric,em}$), the external load connected to the starter motor (T_{load}) and the inertia of the motor (J_{em}). In a model ω_{em} would be a state and there would be 2 unknown model parameters of this model, the friction $T_{fric,em}$ and the inertia J_{em}. The external load on the motor is provided through its connection to the ICE.

In the modelled cranking system the starter motor is connected to the ICE through a ring gear and a pinion [22]. These components provide a ratio between the torque of the starter motor and the ICE. The pinion of such a system is a small gear with few cogs. When the rotational speed of the pinion is equal to or bigger than the rotational speed of the ring gear the pinion is stiffly connected to the ring gear. When the speed of the pinion drops below the speed of the ring gear the pinion disconnects. This is in order to prevent the starter motor from acting as a load on the ICE after ignition. The ring gear is a large gear on the outside of the flywheel of the ICE. This gives the relationship in (3.18) and (3.19) between the torques and rotational speeds of the rotating bodies.

$$T_{em,ice} = K_g T_{em} \tag{3.18}$$

$$\omega_{em} = K_g \omega \tag{3.19}$$

$T_{em,ice}$ denotes the torque delivered from the starter motor to the ICE via the ring gear and in (3.19) ω denotes the rotational speed of the ICE. In both (3.18) and (3.19) K_g is the gear ratio of the system's ring gear. A common configuration on the Scania engines uses 158 cogs on the ring gear and 12 on the pinion, giving a gear ratio of $K_g = 158/12 \approx 13.17$.

3.2.1 Used Variations of the Starter Motor Model

As mentioned in the introduction to Chapter 3 there are two different cranking models used in this thesis, Model 1 and Model 2. Their differences in their starter motor submodels are explained here. The starter motor model is one but not the only thing separating the two models. In Model 1 the model equations of the starter motor contain three model constants, κ_{em}, R_{em} and L_{em} that need to be parametrized together with the parameters of the ICE model. The model uses one internal state in the output equations, the circuit current I. The circuit current also forms one of two outputs of the model, the other being the torque applied to the ICE crankshaft, T_{em}. The inputs to the model are the voltage applied to the electric motor by the battery, U_b and the rotational speed of the motor, ω_{em}. Since the motor is connected to the crankshaft of the ICE, ω_{em} is considered the same as the rotational speed of the ICE [12] [11]. Any gear ratio in Model 1 is aggregated into the model constant of the electric motor, κ_{em}. The starter motor inertia of Model 1 is considered part of the inertia of the ICE, presented in Section 3.4. This means that for Model 1 the electrical dynamics of the starter motor are separately modelled, while the mechanical properties are aggregated with the mechanical properties of the ICE.

In Model 2 the electric dynamics of the starter motor circuit are considered as a fast process in relation to the other dynamics. This means that the inductance of the circuit is eliminated, as is the dynamic current equation (3.16). This means that the current is calculated linearly at each time instant instead of having an internal state for any non-linear dynamics. Instead Model 2 includes the mechanical dynamics of the starter motor and the ratio of the pinion and ring gear. If we make the assumption that the rotational speed of the pinion will never drop below the relative rotational speed of the ring gear the two rotating masses of the starter motor and the ICE are thus connected. This means that the rotational speeds, inertias and governing equations can thus be aggregated using the method presented in Chapter 10 of [11]. This gives the governing equation of the rotating masses of (3.20).

$$\dot{\omega} = \frac{K_g(T_{em} - T_{fric,em}) - T_{load,ice}}{J} \tag{3.20}$$

In (3.20) the term J denotes the combined inertias of the starter motor and the ICE, with compensation for the ring gear between them. The expression for J is presented in (3.21).

$$J = J_e + K_g^2 J_{em} \tag{3.21}$$

In summary the starter motor model configuration of Model 2 uses four model constants, κ_{em}, R_{em}, $T_{fric,em}$ and J. There is no state for the electrical dynamics of the motor. The rotational speed of the electric motor (ω_{em}) is modelled, however its dynamics are directly coupled with the dynamics of the ICE, yielding no model state for ω_{em}. The input to the model is the voltage applied to the starter motor (U_b), there are no internal states for the model and the outputs are the torque applied to the ICE (T_{em}) and the current drained from the battery by the starter motor circuit (I).

3.3 ICE Model

This section contains the modelling of the ICE of the cranking model. The aim of this thesis is to model the cranking period of heavy duty truck engines, and therefore this model will be limited to modelling the ICE during cranking before ignition.

3.3.1 Engine Pressure Model

One of the reasons for resistance when cranking a CI engine is the pressure build-up in the cylinders when the engine is cranked. The analytic model applied to this originates from [11] and [10]. We assume for the purpose of this thesis that there are no air leakages in the cylinder during compression and therefore there are no net losses due to pressure build-up. This does however have an effect on the instantaneous behaviour of the engine. Since compression is a non-linear phenomenon there is a need to model the torque applied to the crankshaft at an instantaneous level to model the engine cranking.

The cylinder pressure model uses the crankshaft angle θ to determine the pressure in the cylinders at any instant. The engine modelled is a five-cylinder engine. In such an engine the cylinder rods are placed so that the angle of each cylinder differs with $4\pi/5$ rad in order for the combustion of each cylinder to occur evenly over each complete engine cycle. The constants of the pressure model are all known.

A decision has been made to not model the pressure build-up in the inlet or exhaust manifold since the effects of this are considered small when cranking an engine without ignition. When the engine is merely cranked the increase in pressure due to compression is consumed during expansion and thus there is no net gain in the pressure of the air streaming into the exhaust manifold. In the inlet manifold there is little pressure build-up during cranking since the sucking of the engine at low speed is very small compared to when running at steady state with ignition. A pressure drop in either manifold is possible, though the effects are considered small in this context. If there is a turbo charger on the engine, this is driven by high flow of exhaust gases which require the engine to run with ignition [11]. There is also no modelling of the strangling effect when air flows through the valves in the engine. The airflow is limited and the effects considered small. The pressure inside the combustion chamber of the cylinder, p_{cyl} is a function of the crankshaft angle θ and the ambient air pressure, p_{amb}, that is considered constant at 101 325 Pa, the mean sea level standard atmospheric pressure. When any of the valves in the cylinders are open, either the inlet or exhaust valves, the pressure in the cylinder is modelled as $p_{cyl} = p_{amb}$ [10].

The compression and expansion of air in the cylinder when the valves are closed and the crankshaft is turned is considered adiabatic [11]. As a consequence the pressure and temperature in the cylinder during compression can be described using (3.22), (3.23) and (3.24).

$$p_{cyl} = p_{ivc}\left(\frac{V_{ivc}}{V(\theta)}\right)^{k_c} \tag{3.22}$$

$$\nu_{cyl} = \nu_{ivc}\left(\frac{V_{ivc}}{V(\theta)}\right)^{k_c-1} \tag{3.23}$$

$$p_{ivc} = P_{amb} \tag{3.24}$$

The subscript *ivc* in (3.22), (3.23) and (3.24) means pressure/temperature/cylinder volume when the inlet valve closes. Since the pressure is equal to the atmospheric pressure when the valves are open, p_{ivc} is given as in (3.24). The constant k_c is here taken as 1,3 [10]. Pressure follows the same relation during expansion. The volume $V(\theta)$ is the cylinder volume for the cranking angle θ.

Geometric functions give the cylinder volume as a function of the cranking angle. Some more engine geometry functions gives the torque applied to the crankshaft by the pressure accumulated in the cylinder. Thus we can calculate a torque resistance to engine cranking as a consequence of pressure build-up in the cylinders.

The torque enacted upon the crankshaft by the cylinder pressure is a function of the engine geometry. Using the geometry of the engine it is possible to write a function where the lever from the cylinder to the crankshaft depends solely on the crankshaft angle, θ. The expression in (3.25) provides the orthogonal lever from the force in the cylinder to the crankshaft, $H(\theta)$, describing the torque from the cylinder pressure acting on the crankshaft. In total this gives the expression in (3.26) [11].

$$H(\theta) = a\sin(\theta) + \frac{a^2\sin(2\theta)}{2\sqrt{l^2 - a^2\sin^2(\theta)}} \tag{3.25}$$

In (3.25) a is the engine's crank radius (half of the engine stroke length) and l is the length of the cylinder rod. The lever in (3.25) leads to an expression of the torque from the cylinder pressure on the crankshaft that is presented in (3.26) [11]. In (3.26) the net pressure difference of the cylinder is multiplied by the surface area of the piston head, $\pi B^2/4$ to give the force of the cylinder.

$$M(\theta) = \frac{\pi B^2}{4}(p_{cyl} - p_{amb})\left(a\sin(\theta) + \frac{a^2\sin(2\theta)}{2\sqrt{l^2 - a^2\sin^2(\theta)}}\right) \tag{3.26}$$

In (3.26) B is the cylinder bore of the engine.

3.3.2 Reciprocating Elements

The reciprocating torque is the resistance of the moving components in the engine to change the direction of the piston and is given by Newton's law of motion, $F = ma$. The expression used is:

$$T_r = C_r M_r H(\theta)\ddot{y} = C_r M_r H(\theta)(G_1(\theta)\dot{\theta}^2 + G_2(\theta)\ddot{\theta}) \tag{3.27}$$

Here C_r is a parameter of the model, M_r is the mass of the reciprocating components. H, G_1 and G_2 are geometrical functions of the crankshaft angle. H expresses the orthogonal lever between the piston head and the crankshaft (expressed in (3.25)) and G_1 and G_2 are used in approximating $\ddot{y}$. The acceleration $\ddot{y}$ is the vertical acceleration of the piston head. One can see the approximation being done expressing $\ddot{y}$ as functions of θ, $\dot{\theta}$ and $\ddot{\theta}$. The model originates from [29] with the addition of the scaling parameter C_r. Since the mass and conductance of the reciprocating components are not known here the mass is approximated in M_r and coupled with the scaling parameter to make it possible to fit the data to the model.

3.3.3 Friction Losses

The friction model proposed for this thesis originates from [29]. This model is a development in the structure proposed in [26] and used in [27]. It consists of several components of friction, each representing the friction of the components listed above, piston rings, piston skirts, bearings, valve train and auxiliaries. The total friction torque is denoted T_f and the various components are named T_{f1}, T_{f2} etc. The model structure from [29] also incorporates the dependence of oil viscosity in the different components, thus providing the model with temperature dependence.

Ring Friction Torque

The friction of the piston rings towards the lining of the cylinder is given by:

$$T_{f1} = \eta|H(\theta)|\left[C_{1,fric} + C_{2,fric}|p_{cyl} - p_{amb}| + \frac{B^2(\pi/4)|p_{cyl} - p_{amb}| - M_r G_1(\theta)\dot{\theta}^2}{\eta + G_3(\theta)}\right] \tag{3.28}$$

In this case η is an approximation of the Streibeck diagram to represent the aspect of mixed lubrication between the piston and the cylinder lining. $H(\theta)$ is the geometrical function presented in (3.25) giving the lever between the cylinder and the crankshaft and B is the bore of the cylinder. $G_3(\theta)$ is another geometrical function depending on engine geometry.

The variable z is the hydrodynamic friction coefficient that is given by (3.29). This variable is used when calculating η.

$$z = \sqrt{\frac{\mu\dot{\theta}|H(\theta)|}{L_r}} \tag{3.29}$$

The effect of the motor oil viscosity, μ, on the friction appears in (3.29). L_r is the load on the lubricated area and is expressed in (3.30).

$$L_r = K_1 * \left(K_2 + |p_{cyl} - p_{amb}|\right) \tag{3.30}$$

Using the expressions of (3.29) and (3.30) the coefficient of friction for hydrodynamic lubrication can be obtained through the expression in (3.31).

$$\eta = \begin{cases} c_1 - (c_1 - z)|\sin(\theta)| & \text{for} 1.5\pi \leq \theta \leq 2.5\pi \\ z & \text{otherwise} \end{cases} \tag{3.31}$$

In this equation c_1 is an empirical parameter that is given in [29]. This gives that the ring friction torque can be expressed as a function of engine geometry, oil viscosity and the model parameters $C_{1,fric}$, $C_{2,fric}$, K_1 and K_2.

Skirt Friction Torque

The piston rings are placed on the edge of the piston head and pressing against the lining of the cylinder. The equation in (3.32) describes the friction between the piston skirt and the lining of the cylinder. The piston skirts are the edges of the piston head that is in contact with the lining of the cylinder. Despite the piston rings the edges of the piston head (or skirts) are also at times in contact with the cylinder lining. This gives a friction component for the piston skirts. This component is given by:

$$T_{f2} = C_{3,fric} * \mu\dot{\theta}H^2(\theta) \tag{3.32}$$

The components here are already defined, except for the model parameter $C_{3,fric}$.

Bearings Friction Torque

These equations represent the friction in the bearings of the rotating components, both ends of the piston rod and the camshaft of the engine. These components operate in hydrodynamic friction mode except around the top dead centre (TDC). Around the TDC the oil film between the components is thinner and the lubrication is in the mixed region. The friction component for the bearings in (3.33) is thus valid everywhere except around the TDC.

$$T_{f3} = C_{4,fric} + C_{5,fric}\mu\dot{\theta}G_4(\theta) \text{ for } 0 \leq \theta \leq 1.9\pi \text{ and } 2.4\pi \leq \theta \leq 4\pi \tag{3.33}$$

In (3.33) $C_{4,fric}$ and $C_{5,fric}$ are model parameters and $G_4(\theta)$ is a geometrical function. In a similar way as with the ring friction there is a need for a friction coefficient depending on the mixed lubrication stage of a Streibeck diagram when moving around the TDC, expressed in (3.34).

$$\eta_{bm} = c_2 \left(\frac{\mu \dot{\theta}}{|p_{cyl} - p_{amb}|} \right)^{-1/3} \tag{3.34}$$

The constant c_2 is another empirical parameter presented in [29]. This gives us the bearing friction around the TDC using the expression in (3.35).

$$\begin{aligned} T_{f4} &= \eta_{bm} r_b \\ &* \left[\frac{(\pi/4)B^2 |p_{cyl} - p_{amb}| - a\dot{\theta}^2 M_r \left[\cos\theta + (a/L)\cos 2\theta\right]}{G_5(\theta)} \right] \\ &* |\cos(4.3\pi - 2\theta)| \end{aligned} \tag{3.35}$$

In 3.35 $G_5(\theta)$ is a known geometrical function. To summarize, the bearings friction torque is computed using (3.33), (3.35) and (3.36).

$$T_{f34} = \begin{cases} T_{f3} & \text{for } 0 \le \theta \le 1.9\pi \text{ and } 2.4\pi \le \theta \le 4\pi \\ T_{f4} & \text{for } 1.9\pi \le \theta \le 2.4\pi \end{cases} \tag{3.36}$$

Valve Train Friction Torque

This model accounts for the friction in the cam/follower, rocker arm/pivot shaft, camshaft bearings, valves/valve guides and seals. The valve train friction exists over the engine's entire speed range. It is expressed in (3.37) and scales with the engine speed.

$$T_{f5} = C_{6,fric} * (1 - c_3\dot{\theta})|H(\theta)| \tag{3.37}$$

Here is another model parameter, $C_{6,fric}$, and an empirical parameter presented in the article, c_3 [29]. The parameters listed in [29], c_{1-3}, deal with the mode of friction and lubrication at three different points in the friction model. These have been fitted for a smaller diesel engine than the one modelled in this thesis. The difference in lubrication modes does not differ greatly between different engine sizes since the manner of lubrication is similar between diesel engines of this type [11].

Auxiliary Torque Losses

This section contains a model of the friction losses in auxiliary components such as unloaded journal bearings, water pump, fuel pump, oil pump and generator. A hydrodynamic lubrication model is assumed, that uses one parameter, $C_{7,fric}$, to scale this friction. The expression is given in (3.38).

$$T_{f6} = C_{7,fric} * \sqrt{\mu\dot{\theta}} \tag{3.38}$$

The reason that the oil viscosity, μ, is included in the auxiliary losses expression in (3.38) is that all auxiliaries driven by the crankshaft are lubricated in some fashion and this effect is aggregated in this variable.

Motor Oil Viscosity

Finally, there is a need for a model of the viscosity of the motor oil used in many of the friction equations above. Normally in modelling this viscosity is determined from empirical models or look-up-tables. This model uses the same one that is used in [29], since it is made to model the viscosity in the operating range of the model used, from the cold temperatures at around -20°C to the warm at +35°C. The oil viscosity depends heavily on the temperature of the motor oil, ν_{oil}, and it is through this model that the temperature dependence in the model is achieved. The empirical model is given in (3.39).

$$\mu = 7.849 * 10^{-5} * \exp\left(\frac{-8.670 * 10^{-3} T_{oil}^2 - 1.153 T_{oil} + 1361}{T_{oil} + 133}\right) \tag{3.39}$$

3.3.4 Comment On the Friction Model

When comparing the different models presented in this chapter it is easy to see that the majority of model parameters in need of estimation stems from the friction model. There are a few reasons for this. Firstly the base of the friction model proposed here is an instantaneous friction model based on physical properties of the engine. As mentioned, the base of the model stems from [29]. This model requires very detailed information on the components and composition of the engine that is to be modelled. This information is not available for the purpose of this thesis and thus a lot of constants that would not need to be estimated with the information available must now be estimated.

It is stated in [29] that the friction components modelled in the article and this chapter contribute each to a certain percentage of the total friction. The ring friction provides 40.3%, the skirt friction provides 15.7%, the bearings friction 29.1%, the valve train 8.8%, and the auxiliary losses account for 6.1% during cold start conditions.

As mentioned in Section 3.2 there are two different models used in this thesis, Model 1 and Model 2. These two models differ in the starter motor models used, presented in Section 3.2, and in the friction model used. Model 1 uses all of the friction components mentioned in this section while Model 2 uses all but (3.37) and (3.38). Since these two components are meant to contribute with only 14.9% of the total friction when the model is well calibrated the attempt is made to model the cranking without the use of these two components in Model 2. The reason for this is to reduce model complexity and reduce the number of model parameters that need estimating. This is addressed when comparing the results of evaluating the two different models.

3.3.5 Summing Up the ICE Model

In total, the states used by the ICE are the motor oil temperature (ν_{oil}) and the crankshaft angle and its two derivatives (θ, $\dot{\theta} = \omega$ and $\ddot{\theta} = \dot{\omega}$). The model parameters of the ICE model are used in the models for representing losses due to reciprocating elements and friction. Since compression is considered adiabatic the compression relations are known functions of the engine geometry and crankshaft angle, angular speed and angular acceleration. The modelling parameters are C_r, K_1, K_2 and $C_{1-7,fric}$. All of these except C_r are used in the friction model.

In summary the ICE model consists of three major components, the pressure losses, the reciprocating losses and the friction losses. These three contribute to the total losses in the engine.

3.4 Model Summary

The ICE model couples the driving torque of the electric motor with the losses due to compression, reciprocating elements and friction. The governing equations differ between the two different models. The governing torque equation describing the change in crank angle acceleration, $\ddot{\theta}$, for Model 1 is given by (3.40). It is a general model for rotational acceleration and the principle is presented in [20].

$$\ddot{\theta} = \frac{T_{em} + T_r + T_p - T_f}{J_e} \tag{3.40}$$

Where J_e is the inertia of the rotating parts of the engine. It includes the rotating masses of the electric motor and the engine's crankshaft. Since these are connected during cranking they will mechanically act as one connected, rigid mass. Thus the rotational speed of the ICE is the same as the rotational speed of the electric motor, $\omega_{em} = \omega$. Therefore the inertia of the components can be added up to one total inertia. The total friction losses, T_f, are given by the summation of the above explained friction components in (3.41).

$$T_f = T_{f1} + T_{f2} + T_{f34} + T_{f5} + T_{f6} \tag{3.41}$$

Since the expression in (3.27) depends on the angular acceleration of θ there is a need to rewrite the expression above as in (3.42).

$$\ddot{\theta} = \frac{T_{em} + T_p - T_f + C_r M_r H(\theta) G_1(\theta) \dot{\theta}^2}{J_e - C_r M_r G_2(\theta)} \tag{3.42}$$

The ICE model uses three model states, the crankshaft angle θ, the crankshaft angular speed $\dot{\theta}$ and the oil temperature T_{oil}. Since the lubrication oil of the ICE is pumped from the oil capacity pan, the temperature of the motor oil during cranking is the same as the oil temperature in the pan. Because no ignition takes place during cranking and cranking only lasts at the most 20 seconds, there is no increase in oil temperature during cranking [12]. Since the aim here is to model the engine cranking during cold start, the oil temperature is set to the same value as the ambient temperature.

The starter motor model and ICE model in Model 1 include four states, one for the crank angle (θ), one for the crankshaft rotational speed ($\dot{\theta} = \omega$), one for the current through the starter motor armature (I) and one static state for the ambient temperature (ν_{amb}). All of the factors in the models can be expressed as functions of these states. The two models have 14 model parameters between them, κ_{em}, R_{em}, L_{em}, J_e, C_r, K_1, K_2 and $C_{1-7,fric}$. These are the model parameters and states used by Model 1.

The mechanical equation for Model 1 in (3.40) is not the same as the one used in Model 2. The derivation of the one used in Model 2 can be found in Section 3.2. Since Model 2 uses two fewer friction components than Model 1, the expression for the friction of Model 2 becomes (3.43).

$$T_f = T_{f1} + T_{f2} + T_{f34} \tag{3.43}$$

Coupling (3.20) with the expressions for the load torques of the ICE presented in Section 3.3 this yields a governing mechanical equation for Model 2 in (3.44).

$$\ddot{\theta} = \frac{K_g * (T_{em} - T_{fric,em}) + T_p - T_f + C_r M_r H(\theta) G_1(\theta) \dot{\theta}^2}{J - C_r M_r G_2(\theta)} \tag{3.44}$$

In (3.44) the effects of the ring gear ratio K_g, the constant friction of the electric motor $T_{fric,em}$ and the aggregated inertia J are demonstrated. This means that Model 2 uses one less state than Model 1 since no electrical dynamics are considered. Otherwise the used states are the same and Model 2 has got 12 modelling parameters, κ_{em}, R_{em}, $T_{fric,em}$, J, C_r, K_1, K_2 and $C_{1-5,fric}$.

4

Parameter Estimation and Model Evaluation

This chapter treats the fitting of the described models to the data provided for the purpose of this thesis. It includes a discussion on the data available to set the parameters of the models, the method used for this and the different parameter estimations that have been made for this model.

The models are defined in Chapter 3, and the *System Identification Toolbox* in *Matlab* is used to fit the models to the data [21]. The toolbox includes functions to fit the model output to data by estimating the model parameters.

4.1 Grey-Box Estimation Using Data

The data made available by Scania for the purpose of this thesis has been introduced in Section 2.4. Each measured quantity is given as a series of values over time, and is then defined as an iddata-object consisting of measured signals of a system's input and output.

Since each of the models in Chapter 3 is a non-linear model, the *Matlab* model class idnlgrey is used. The class is included in the above mentioned toolbox and is developed to handle non-linear models. The grey-box models have the structure of the modelled system, but has got tuning parameters in order to fit the model to the data. The states and parameters of each model are listed in Sections 4.2 and 4.3. The factors separating each of the data sets are considered known in each case due to measurements, namely the temperature and battery SOC. From these known parameters it is possible to calculate the initial value of all model states since the SOC gives a measure of the extracted charge of the battery which is one model state and the temperature of the entire system is equal to the ambient temperature during cold starting.

The *System Identification Toolbox* includes commands to estimate the unknown parameters using a prediction error minimization algorithm. This estimation iteratively sets the model tuning parameters. The toolbox uses the solver ode45 to solve the continuous differential equations that form the model. This solver uses a variable step length when solving differential equations. The method used for estimating the parameters is the prediction-error minimization algorithm using the non-linear least-squares method, which gives the cost of the estimation at every iteration as the square of the difference between the measured and simulated outputs [21] [19]. This enables the toolbox to estimate the tuning parameters of non-linear models such as the ones in this thesis.

The data series contain measured signals during cranking at different temperatures. The data is divided into series, each starting with a fully charged starter battery. The engine is then cranked until ignition occurs and then shut down to prevent heating of the components. The entire system is then allowed to cool and then the cranking is repeated. Between the engine starts the battery is drained to a lower SOC. This gives a series of measurements of engine cold starts [23]. The content of the data series differ since not all measured variables are present in every series. The measurements have been made with a frequency of 5000 Hz. A plot of typical data collected at 0°C can be seen in Figure 2.8. An overview of the measured variables in the data series is presented in Table 4.1. There is no information available on the exact SOC embedded in the data sets. When the data was originally collected and compiled by Scania several plots were made where measured data was presented as a function of extracted charge from the battery. From these plots the SOC has been roughly estimated. This should not alter the viability of the model but in a future recalibration there would be need for more exact SOC data.

Table 4.1: *Variables available in the cranking data.*

Variable	**Unit**	**Comment**
Cranking current	[A]	Battery model input signal
Battery voltage	[V]	Battery model output signal
Starter motor voltage	[V]	
Engine rotational speed	[rpm]	The physical property to be modelled in this thesis
Ambient temperature	[°C]	
Starter motor brush temp	[°C]	
Starter motor stator temp	[°C]	
Engine block temp	[°C]	Varies no more than 2 °C during cranking
Sample rate	[Hz]	5000 Hz in all cases used for model evaluation, see Section 2.4

4.2 Battery Model Parameter Evaluation

As listed among the data variables in Table 4.1 two of the measured variables present in every data series are the battery current and voltage. From a causality viewpoint these two are considered as the input and output of the battery model [14] [20]. Therefore these two measurements will be used to correctly set the parameters of the battery model. In earlier parametrizations of this battery model made in [16] and [24] the aim has been to parametrize the model to fit a regular car battery, differing from a heavy duty truck battery in some aspects. The parameter values determined in these studies serve as the initial guess of the parameters estimated for the model in this thesis. Thus the parameters of the heavy duty truck battery are estimated with the parameters of the car battery as starting point. In [16] and [24] data has also been collected to correctly model the charging of the battery. Since the aim of this thesis is to model the cranking this will not be done in this thesis.

It is important when evaluating the estimation of the battery parameters to consider the final aim of this thesis. The aim is not necessarily to correctly model the subsystems making up the cranking systems of a heavy duty truck, but to correctly model the final process of cranking. This means that the model validation is done with respect to the simulated rotational speed of the ICE in the cranking model. It is not considered a problem if the internal signals of the cranking model do not fit their measured counterparts. With this in mind, the dynamics of the system known in the grey-box model structure are viable only if the internal signals are realistic. Therefore it is important that the parameters provide a battery model capable of discharging in a similar way to a real battery, if not exact, and to follow the same characteristics for the output change as a consequence of varying SOC and battery temperature. If these criteria are met by the parametrized model, the model fulfils its purpose.

4.2.1 Estimation

The parameter estimation is made on an $2.4GHz$ Intel Xeon processor with 8 GB RAM. Out of the 113 data sets available 22 have been selected for parameter estimation, 4 from each cold start temperature except for $+10C$ where 2 are selected. This is because there are fewer data sets available at $+10C$. As the cost of the model error is iterated and reduced as the model is fitted to the data during parameter estimation it is allowed to reduce for as long as it keeps significantly improving. If the cost stabilizes at a certain level during the estimation, the estimation is stopped since it is assumed that there is no significant gain in continuing, even if the fit between model and data is not considered good. This is done in order to not waste computation time. The model estimation time for each of the 22 data sets can be seen in Figure 4.1.

The model estimation for each data set is done individually because we are estimating a model of the dynamics of the system in each case. Also, the individual estimations makes it possible to choose the number of data sets used during each estimation.

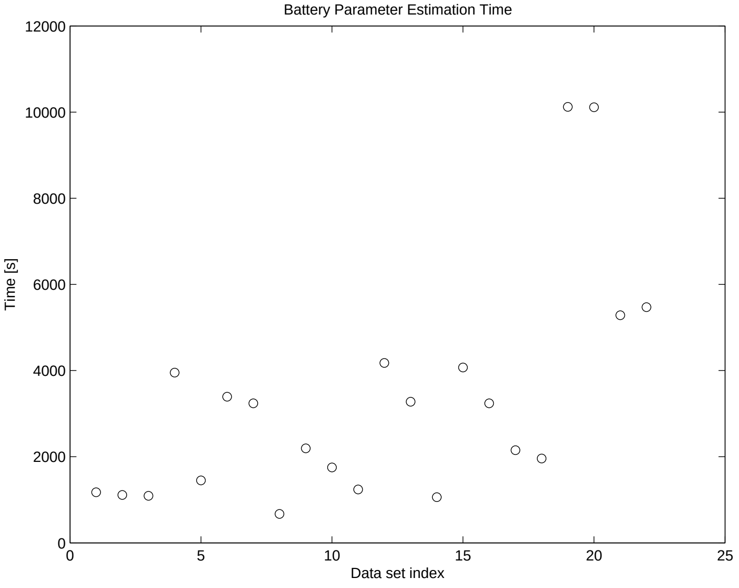

Figure 4.1: *A plot of model parameter estimation time for each data set used to estimate the battery model parameters.*

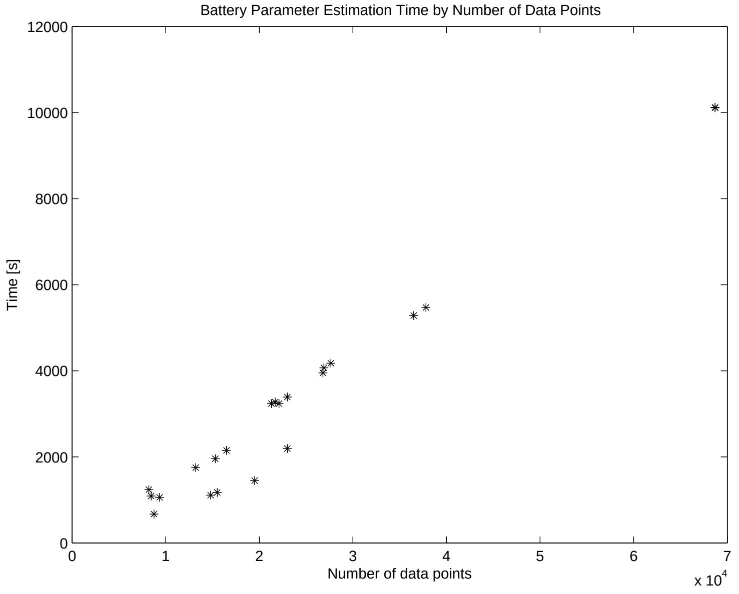

Figure 4.2: *A plot of the battery parameter estimation time as a function of the number of ponts contained in the data set used for the estimation.*

Since the estimation algorithm evaluates the model input and output at every data point the time needed to fit the model to the data scales with the number of data points in the data set. Figure 4.2 contains a plot of model estimation time as a function of data set length.

In Figure 4.2 it is shown that the estimation time scales linearly with the number of data points. For each data set the five battery model parameters are estimated. As listed in Section 3.1 the parameters are the EMF constant K_e, the two terminal resistance constants R_{00} and Ao, the parallel resistance constant R_{10} and the capacity time constant τ_1. In Figure 4.3 the estimated values of each of these parameters is plotted for each data set used.

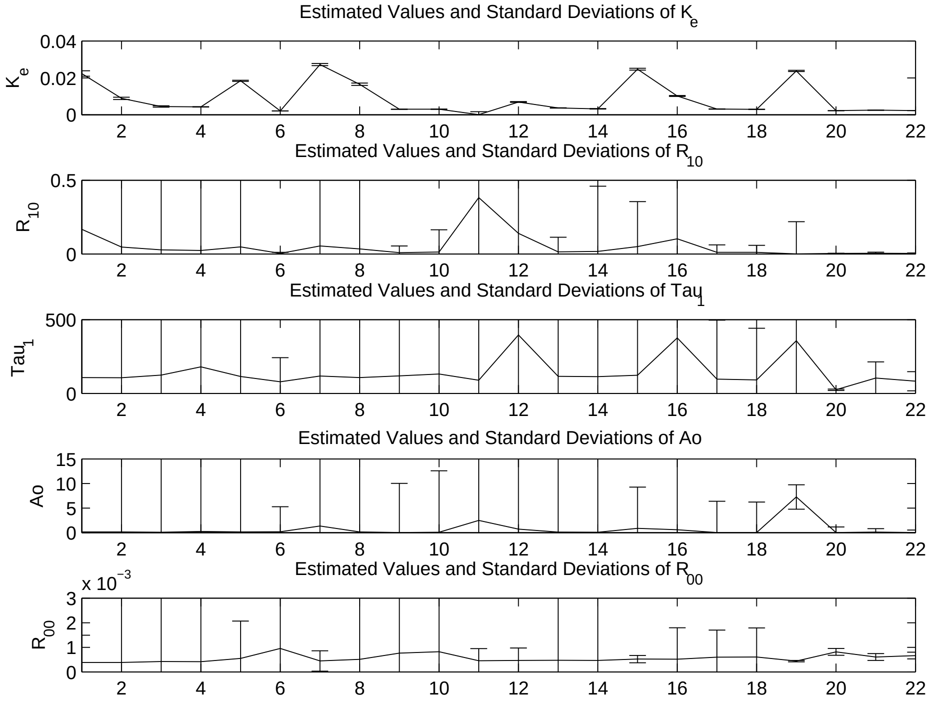

Figure 4.3: *A plot of the estimated values and standard deviations of the battery parameters for each data set used for the battery parameter estimation. Parameter values are plotted as a continuous line varying with the data set index. The standard deviation is marked as an orthogonal line at each parameter valiue.*

For each estimated parameter value in Figure 4.3 the estimation algorithm has determined the estimated standard deviation of that value. The standard deviation of each model parameter for each data set is plotted adjacent to the corresponding parameter value in the same plot.

Since the aim is to estimate model parameters that are valid for each data set the estimated parameter values are to be weighted together to determine the general parameters. For this (4.1) is used. The expression in (4.1) weighs each estimated parameter value by the certainty of the estimated value, the variance [20]. The variance is the square value of the standard deviation and is thus also provided by the parameter estimation.

$$\hat{\theta} = \frac{\sum \frac{\hat{\theta}_i}{\sigma^2_{\theta_i}}}{\sum \frac{1}{\sigma^2_{\theta_i}}} \tag{4.1}$$

In (4.1) $\hat{\theta}$ is the estimated general parameter value for each battery model parameter, θ_i is the parameter's estimated value for data set i and $\sigma^2_{\theta_i}$ is the variance for the same parameter and data set. Estimated parameters with lower certainty are thus given a lower weight in the general parameter values. Under the assumption that each parameter is estimated separately and there is no dependence between different estimations the variance of the estimated parameter can be given by (4.2).

$$Var(\hat{\theta}) = \frac{1}{\sum \frac{1}{\sigma^2_{\theta_i}}} \tag{4.2}$$

The components of (4.2) are introduced above. The estimated and weighted parameter values and their standard deviations are presented in Table 4.2. Since the standard deviation is the square root of the variance it is indirectly given by (4.2) for each weighted parameter.

Table 4.2: *Estimated parameter values for the battery model using* (4.1).

Parameter	**Value**	**Std. Dev.**
K_e	0.0024	1.026e-5
Ao	0.0041	0.389
τ_1	24.9918	4.546
R_{10}	0.2152	7.611e-4
R_{00}	0.0005	2.766e-5

As can be seen by the uncertainty levels of Figure 4.3 the values of K_e, R_{00} and R_{10} are generally considered certain. The estimator has managed to estimate these to a low error.

4.2.2 Verification

When the model parameter estimation has been made for the battery model different data sets are used to verify the estimated model. The parameters presented in Section 4.2.1 are therefore implemented as the fixed parameters of the battery model of the same type used for the estimation. After this a number of data sets are used to verify the input-output correlation for each of them. These data sets are not the same sets used for estimation of the model but sets containing the same elements. For each data set the measured battery current is used as input to the battery model with the estimated parameters and the measure voltage is considered the reference signal for the model output. For model validation 11 data sets are used, two from each temperature level and one from $+10C$ since there are fewer data sets at this temperature. The model output is then compared to the measured battery voltage that is an output, in order to verify that the battery model can produce sufficient model accuracy for the purpose of this thesis.

Figures 4.4 to 4.9 contain plots of the measured battery current, simulated voltage and measured voltage for six of the verification data sets mentioned above. The six verifications differ in temperature and SOC. As mentioned in Section 4.1 the SOC is an approximation in each case. The reason for demonstrating six out of eleven verification sets is to save space in the report. All eleven sets are considered when drawing the conclusions on the model evaluation.

In general there is good model accuracy in the verification simulations in Figures 4.4 to 4.9. There is a slight drift tendency over the course of the cranking, clearly visible in Figures 4.5, 4.6 and 4.8. This could be due to the inaccurate SOC values for the estimation and verification data. If the information on SOC change over the course of several crankings is inaccurate it could lead to inaccurate model behaviour when charge is extracted during a cranking period. The effect of SOC on battery EMF can be seen in Section 3.1. The drift could also be the result of a dynamic behaviour in the battery that the current model structure is unable to represent or a flaw in the battery model.

In the simulations of Figures 4.4 to 4.9 the general dynamics are sufficient for the purpose of this thesis and the voltage delivery by the battery model is in the correct area, with realistic values and dynamics. The battery model with the estimated parameters of Table 4.2 will be used for the remainder of the thesis for both Model 1 and Model 2. Its implementation will be the same for both models.

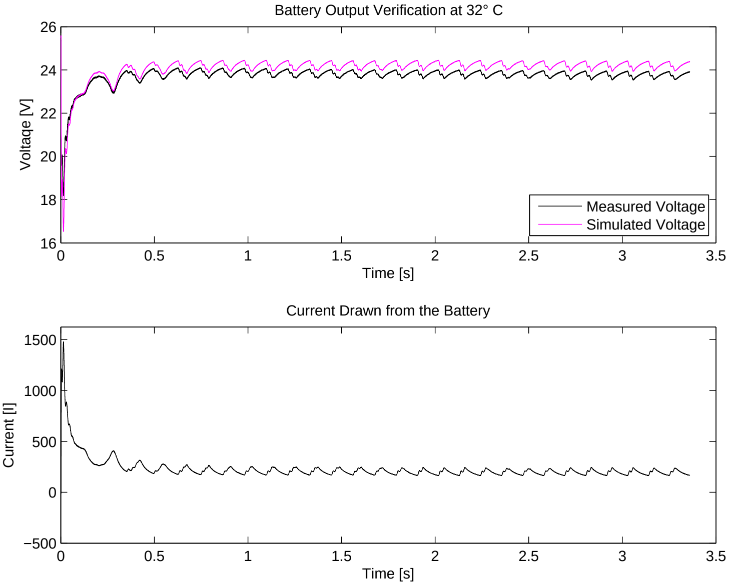

Figure 4.4: *Verification plot of the battery model simulated at +32°C.*

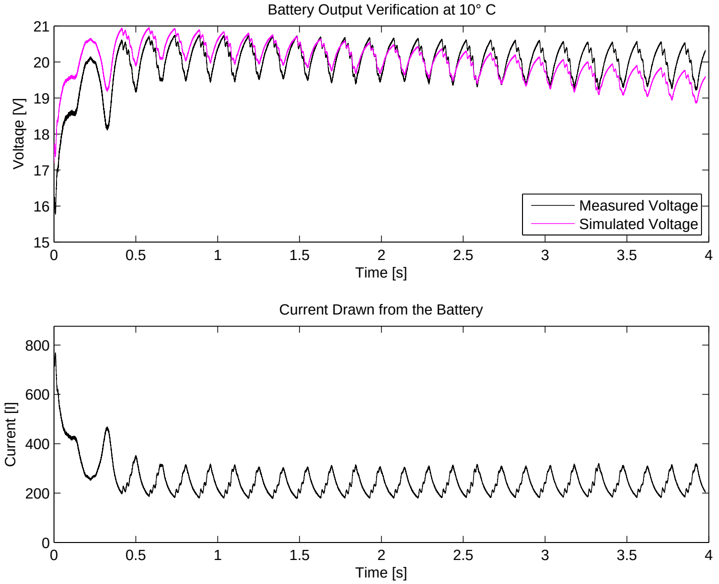

Figure 4.5: *Verification plot of the battery model simulated at +10°C.*

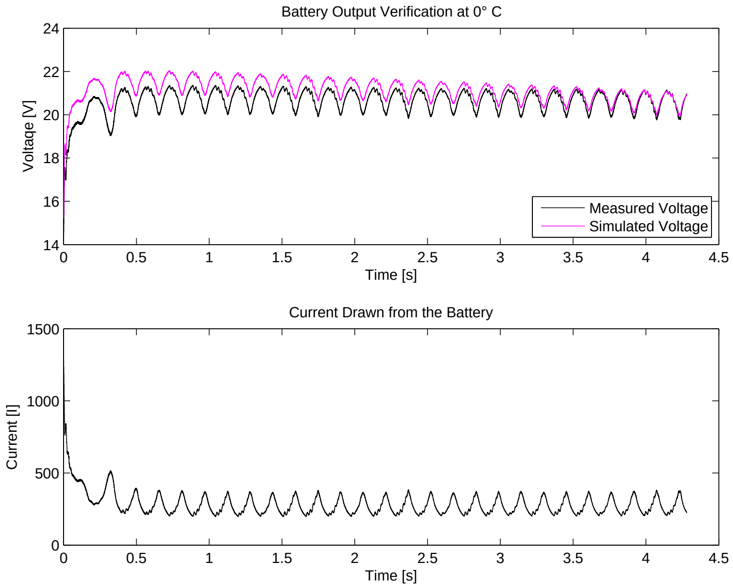

Figure 4.6: *Verification plot of the battery model simulated at* $0°C$.

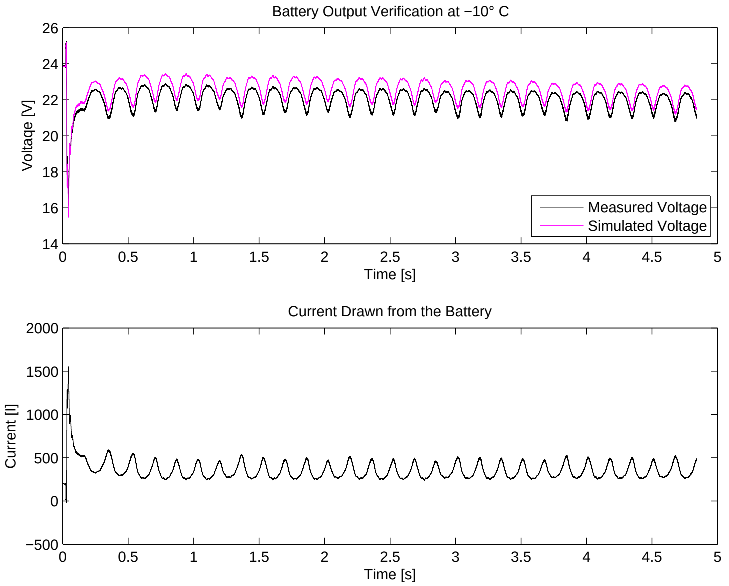

Figure 4.7: *Verification plot of the battery model simulated at* $-10°C$.

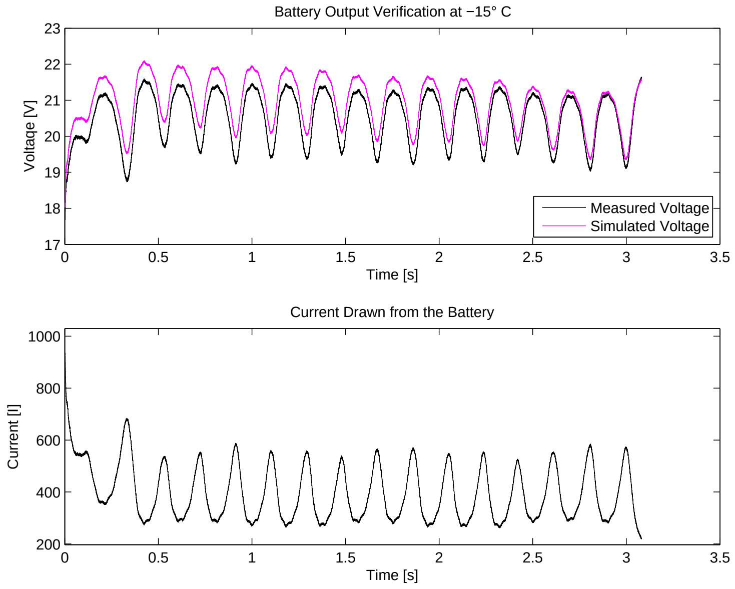

Figure 4.8: *Verification plot of the battery model simulated at* $-15°C$.

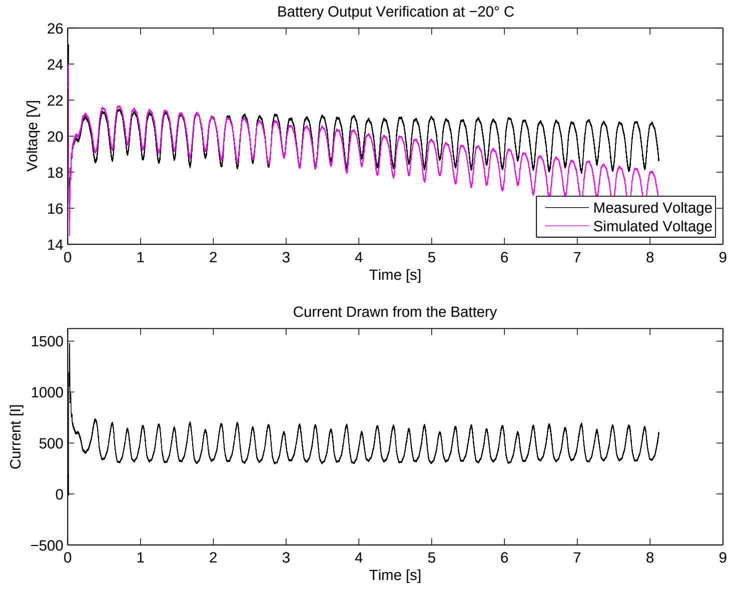

Figure 4.9: *Verification plot of the battery model simulated at* $-20°C$.

4.3 Cranking Model Parameter Evaluation

The estimation and validation of the cranking models use data series of the same type as listed in Section 4.2. The cranking models include the battery model parametrized in Section 4.2, but the parameters estimated throughout that section are not estimated in the cranking model. Since the battery model is the same for both Model 1 and Model 2, these use exactly the same equations and parameters to represent the battery. The two cranking models include the states and model equations in the battery model, but adds the states and model equations of the starter motor and ICE models. The parameters that are to be evaluated in this chapter are the ones introduced in Sections 3.2 and 3.3. The parameters are listed in Table 4.3.

Table 4.3: *A list of the parameters that need estimating for Model 1 and Model 2.*

Model 1	κ_{em}	J_e	C_r	K_1
	K_2	$C_{1,fric}$	$C_{2,fric}$	$C_{3,fric}$
	$C_{4,fric}$	$C_{5,fric}$	$C_{6,fric}$	$C_{7,fric}$
	R_{em}	L_{em}		
Model 2	κ_{em}	J	C_r	K_1
	K_2	$C_{1,fric}$	$C_{2,fric}$	$C_{3,fric}$
	$C_{4,fric}$	$C_{5,fric}$	R_{em}	$T_{fric,em}$

4.3.1 Estimation

The estimation of the cranking models' parameters has been made on a system similar to the one described in Section 4.2.1. Thus the time and performance of the estimation are comparable between the two models. As stated, the battery model with its estimated parameters forms part of the cranking model though the parameters of the battery model are kept fixed during parametrizing of the cranking model. Thus the battery model parameters are not estimated here. The same 22 data sets that were selected for the battery estimation are now used for the cranking model estimation. These sets are the ones presented in Section 4.2.1 and not the data sets used for verification in Section 4.2.2. Figure 4.10 contains the estimation time of both Model 1 and Model 2 as a function of the data set length, similar to the plot in Figure 4.2 for the battery model.

One can see in Figure 4.10 that the linear relationship between estimation time and data set length that holds for the battery model is not valid for the cranking models. It seems that when the complexity of the model increases the dominating factor in the estimation times is no longer the data set length but the non-linearities and the high number of parameters in the model. It is also worth mentioning that the relationship between data set length and parameter estimation time present in these models is not general. In a general parameter

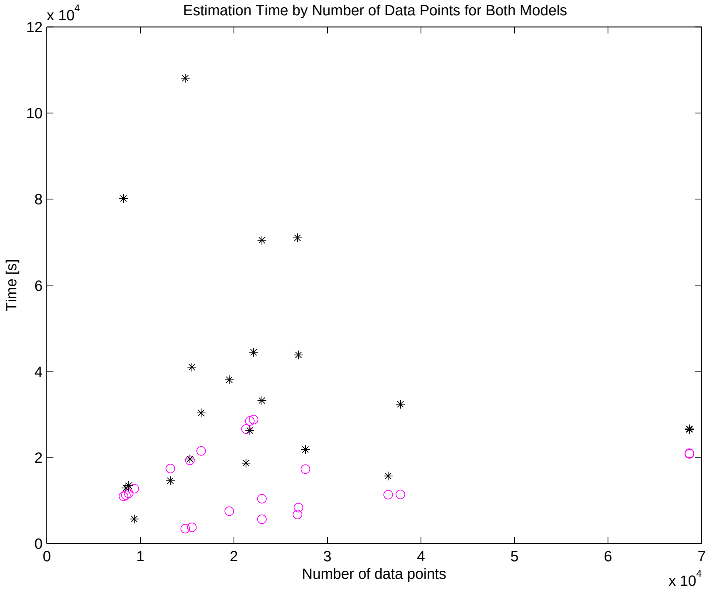

__Figure 4.10:__ A plot of the parameter estimation time for Model 1 and Model 2 as a function of the number of points contained in the data set used for each estimation. Model 1 estimation times are plotted with darker star symbols and Model 2 estimation times are plotted with brighter circles.

estimation of this sort data that can easily be reproduced by the model can give an easier cost function and result in lower estimation times than shorter data sets that are not as easy for the model to reproduce.

The number of parameters that need estimating in both models here is significantly higher than for the battery model, twelve or fourteen parameters compared to five parameters for the battery model. The number of states for the two cranking models has not increased as much, from five for the battery model to seven or eight for the cranking models. It is however clear that the estimation times for Model 2 are significantly lower than for Model 1. Model 2 cuts the estimation times to about 1/3 of the times measured for Model 1. This could be due to the lower number of parameters, the fewer model states or a generally smoother execution of Model 2.

During estimation of Model 1, two output signals are used for the model, even though the final model is meant to have one. This is to investigate whether adding a measurement signal to what is normally an internal state facilitates the estimator's ability to estimate the model constants. Thus the outputs used are the engine rotational speed in rpm and the current drawn from the battery I. This investigation is possible to do since the current is available in the data sets. Despite two signals being used as outputs during the estimation, the engine rotational speed is the one considered when investigating model fit to data. Like the method presented in Section 4.2.1, the cost of the model error is allowed to reach a stable level during the estimation and then the estimation process is terminated. Figures 4.11 to 4.14 contain plots of the estimated values and standard deviations of the different model parameters of Model 1.

As with the battery model, the estimated standard deviation of each model parameter is used as an indicator of the estimator's certainty in each case. The estimated standard deviation for each parameter and each dataset presented in Figures 4.11 to 4.14 is here plotted adjacent to its corresponding parameter value. In any case where a standard deviation has not been computed for a parameter due to estimation complications the standard deviation of this parameter has been set to the maximum standard deviation of the remaining estimated values of that parameter. This phenomenon can occur due to the complexity of the model and the single output comparison signal.

Throughout Figures 4.11 to 4.14 the variation of the estimated model parameters is generally quite high. In some cases the outlying parameter values correspond with large variation, in other cases the conclusion is that the estimated outlier is certain for the data set in question. The scale of the standard deviation in Figures 4.11 to 4.14 is itself quite varying, and a large uncertainty of some estimated parameter values can be seen. As mentioned the great standard deviation is considered as a sign of uncertainty in the estimated value, reflected in the parameter weighting using (4.1).

The cost function of the prediction error minimization method during the parameter estimation is quite high. It is mentioned in Section 4.2.2 that the cost of the model error is deemed sufficiently low for the battery estimation. This is not the case for the cranking model estimation. The estimator struggled throughout the different scenarios to reach a sufficient level of model fit.

When estimating the model parameters of Model 2 one thing is made differently form Model 1. In order to investigate the benefits of using a measurement signal of an internal model state to estimate the model, the measured current is used as an output signal when parametrizing Model 1, something that is not done for Model 2. Otherwise the same data sets are used when estimating Model 2, and the estimated parameter values and standard deviations are presented in Figures 4.15 to 4.17. There are two reasons for this distinction between the estimations. Firstly, to investigate whether or not this had a significant impact on the model accuracy, and secondly, to facilitate estimating the electric dynamics parameters of Model 1 not present in Model 2.

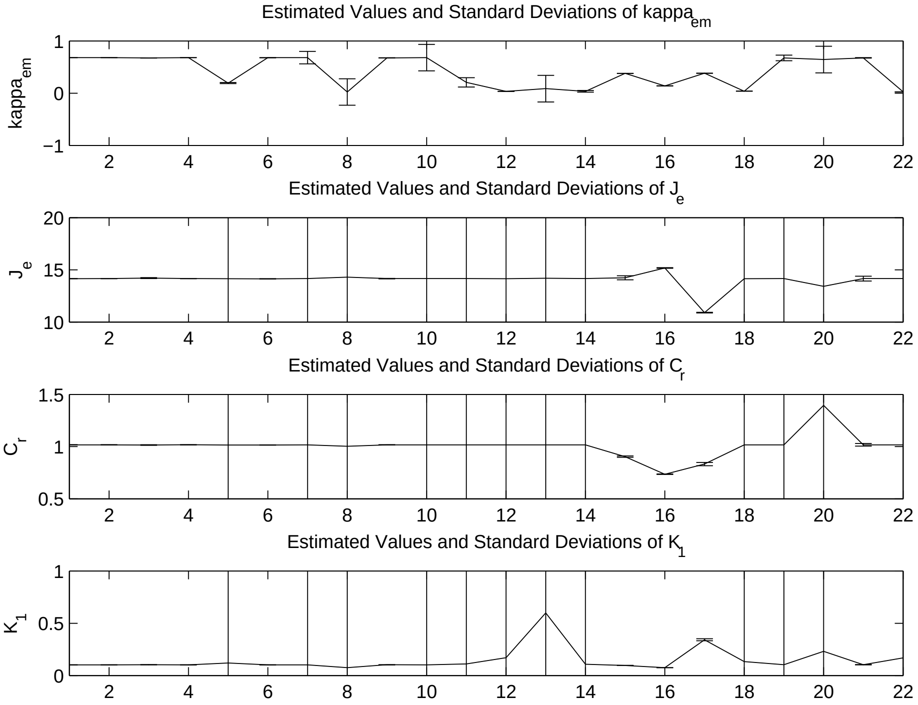

Figure 4.11: *A plot of the estimated values and standard deviations of κ_{em}, J_e, C_r and K_1 for each data set used for Model 1 parameter estimation. Parameter values are plotted as a continuous line varying with the data set index. The standard deviation is marked as an orthogonal line at each parameter valiue.*

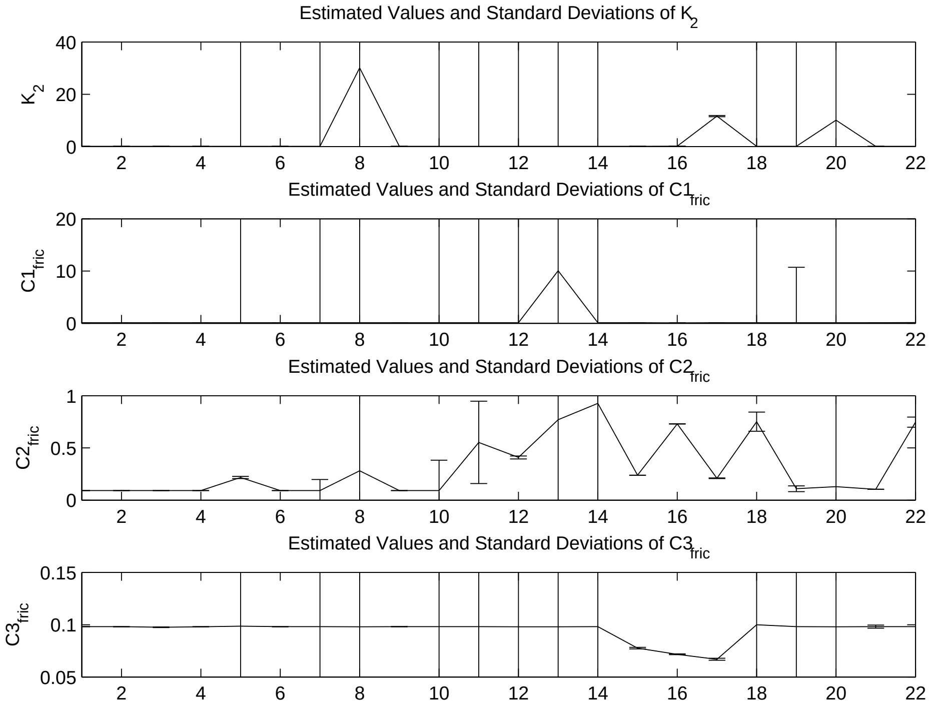

Figure 4.12: *A plot of the estimated values and standard deviations of* K_2, $C_{1,fric}$, $C_{2,fric}$ *and* $C_{3,fric}$ *for each data set used for Model 1 parameter estimation. Parameter values are plotted as a continuous line varying with the data set index. The standard deviation is marked as an orthogonal line at each parameter valiue.*

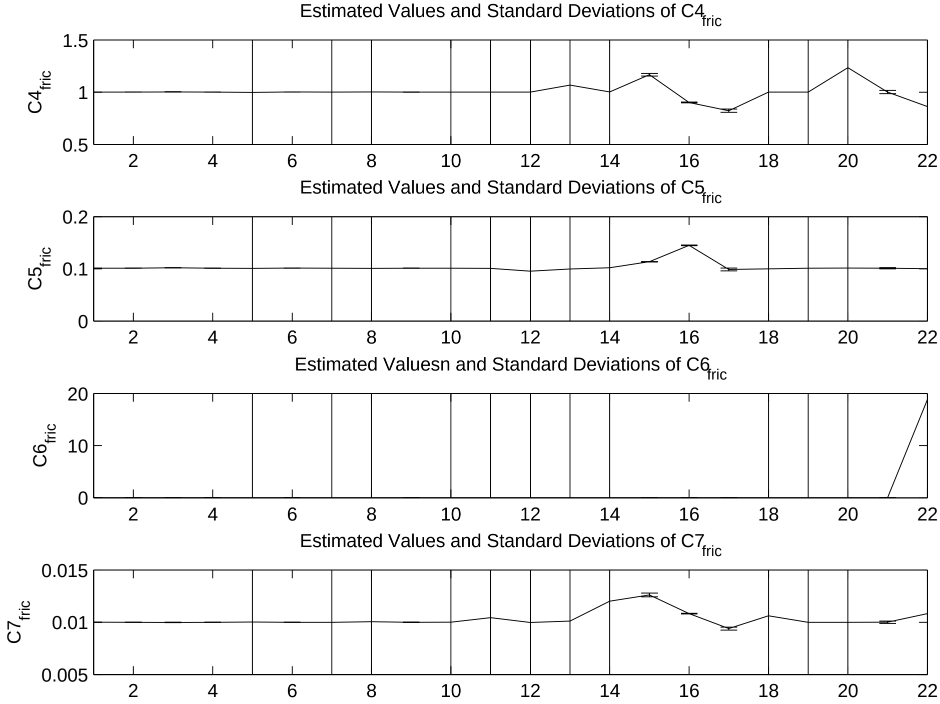

Figure 4.13: *A plot of the estimated values and standard deviations of* $C_{4,fric}$, $C_{5,fric}$, $C_{6,fric}$ *and* $C_{7,fric}$ *for each data set used for Model 1 parameter estimation. Parameter values are plotted as a continuous line varying with the data set index. The standard deviation is marked as an orthogonal line at each parameter valiue.*

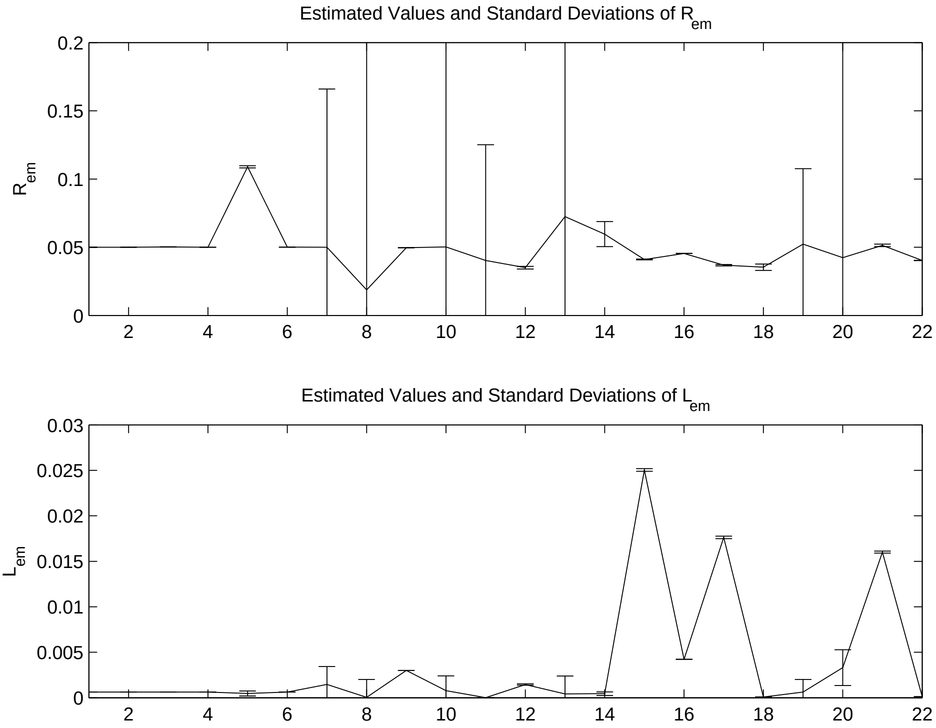

Figure 4.14: *A plot of the estimated values and standard deviations of R_{em} and L_{em} for each data set used for Model 1 parameter estimation. Parameter values are plotted as a continuous line varying with the data set index. The standard deviation is marked as an orthogonal line at each parameter valiue.*

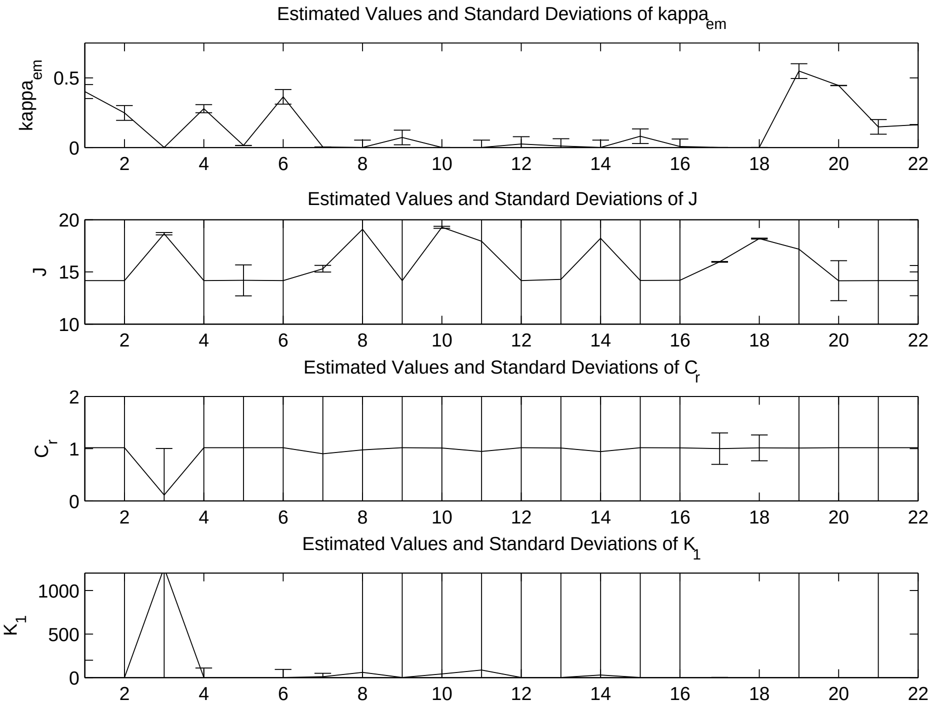

Figure 4.15: *A plot of the estimated values and standard deviations of κ_{em}, J, C_r and K_1 for each data set used for the Model 2 parameter estimation. Parameter values are plotted as a continuous line varying with the data set index. The standard deviation is marked as an orthogonal line at each parameter valiue.*

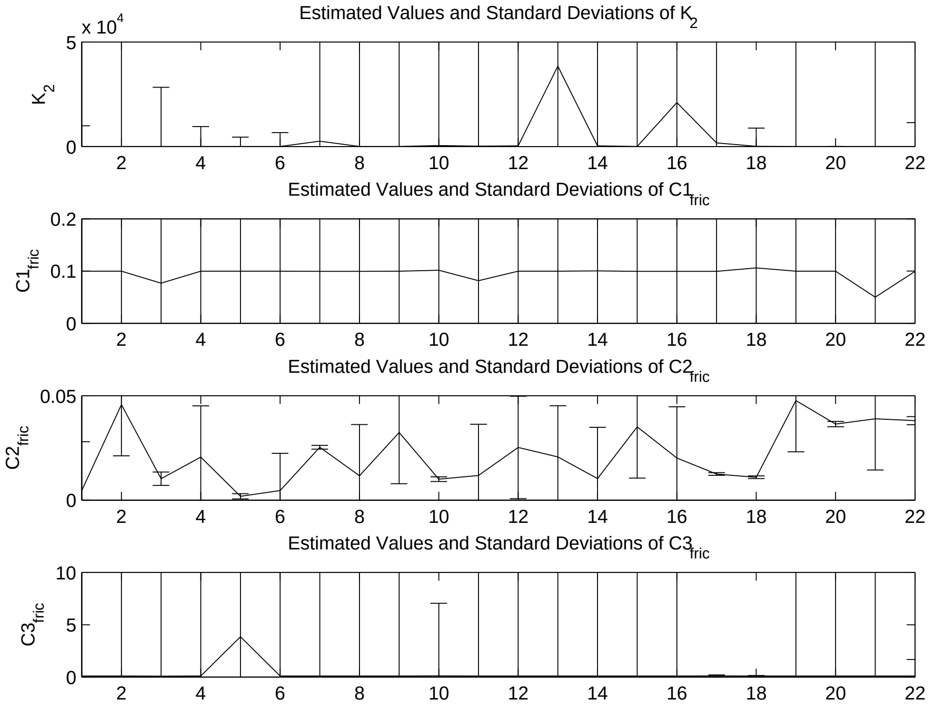

Figure 4.16: *A plot of the estimated values and standard deviations of K_2, $C_{1,fric}$, $C_{2,fric}$ and $C_{3,fric}$ for each data set used for the Model 2 parameter estimation. Parameter values are plotted as a continuous line varying with the data set index. The standard deviation is marked as an orthogonal line at each parameter valiue.*

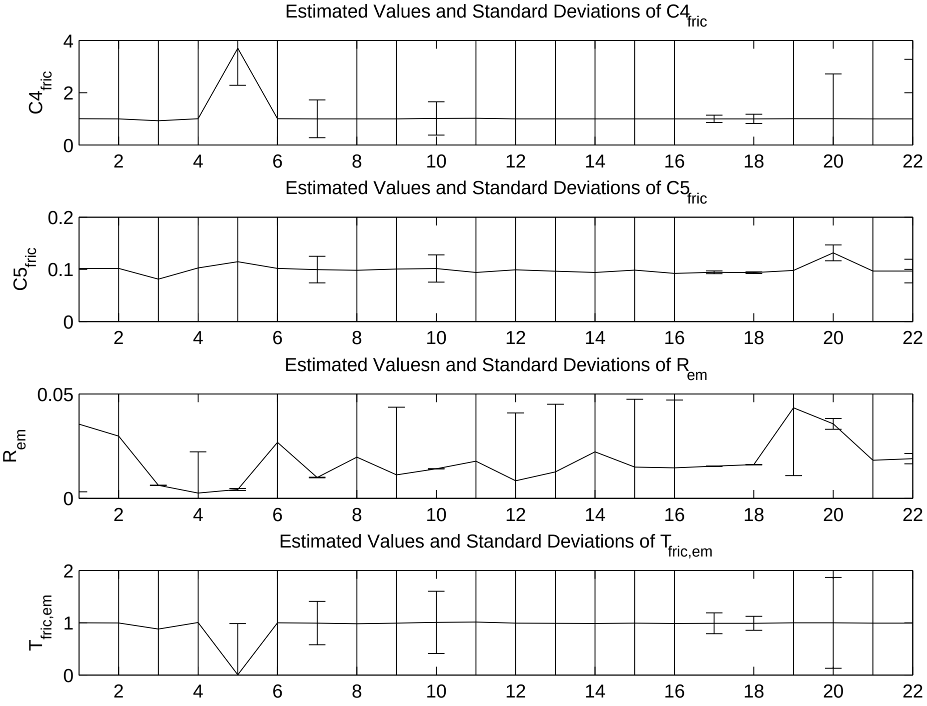

Figure 4.17: *A plot of the estimated values and standard deviations of* $C_{4,fric}$, $C_{5,fric}$, R_{em} *and* $T_{fric,em}$ *for each data set used for the Model 2 parameter estimation. Parameter values are plotted as a continuous line varying with the data set index. The standard deviation is marked as an orthogonal line at each parameter valiue.*

The Model 1 and Model 2 parameters are weighted in the same manner as the battery model parameters, using (4.1). The resulting parameter values and standard deviations are presented in Table 4.4.

When observing Figures 4.11 and 4.15 it is noted that the estimated value of κ_{em} differs largely between Model 1 and Model 2, and the reason for this is that the separate state for starter motor rotational speed included in Model 2 models a higher speed of the starter motor, causing the torque constant to be smaller. The reason for this is that the ring gear and pinion between the starter motor and the crankshaft demands the starter motor to rotate at a higher speed than the crankshaft to deliver the necessary torque. The two rotational speeds differ with a factor of $K_g = 13.17$ since they are connected via the gear, see Section 3.2. The difference in rotational speed between the two rotating bodies is one of the elements added when upgrading Model 1 to Model 2. The corresponding standard deviations of the estimated values in Model 2 are also contained in Figures 4.15 to 4.17, plotted adjacent to the respective parameter value.

Table 4.4: *Estimated parameter values and standard deviations for Model 1 and Model 2.*

Parameter	**Model 1**	**Std. Dev.**	**Model 2**	**Std. Dev.**
κ_{em}	0.4726	1.441e-4	0.003	1.376e-6
J_e / J	14.1112	0.0035	17.1965	0.0273
C_r	1.0133	2.775e-4	0.9708	0.186
K_1	0.1018	2.674e-5	0.4963	0.0135
K_2	0.1011	2.552e-5	0.1018	15.156
$C_{1,fric}$	0.0994	2.736e-5	0.0998	1.684
$C_{2,fric}$	0.0923	2.505e-5	0.0153	3.381e-4
$C_{3,fric}$	0.0979	2.596e-5	0.1018	0.0391
$C_{4,fric}$	1.0003	2.830e-4	1.0143	0.107
$C_{5,fric}$	0.1014	2.569e-5	0.0942	0.0014
$C_{6,fric}$	0.0101	3.105e-6	–	–
$C_{7,fric}$	0.0100	2.745e-6	–	–
R_{em}	0.05	1.344e-5	0.0120	4.167e-5
L_{em}	0	1.689e-7	–	–
$T_{fric,em}$	–	–	0.9795	0.104

4.3.2 Verification

The plots in Figures 4.18 to 4.20 contain the verification plots of Model 1 when simulated at three different temperatures. It is apparent that the model is unable to correctly recreate the measured engine cranking. This could be an indication of that the estimation is too difficult with the increased number of states and parameters that need to be estimated compared to the battery model. The battery model can serve as a measuring stick since it is a non-linear model with five states and parameters, yet the most important factor in its estimation time, as demonstrated by Figure 4.2, is the length of the data set used for estimation. The length of the dataset is of less importance to the cranking models estimation time, as demonstrated by Figure 4.10. Thus the increased complexity of the cranking model causes it to increase its estimation time greatly or there is a factor in the cranking that is not captured by the current model structure.

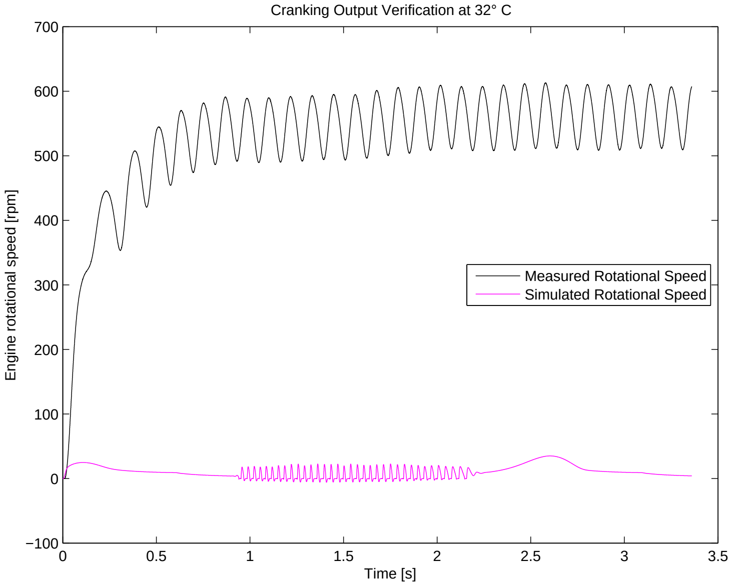

Figure 4.18: *Verification plot of Model 1 simulated at 32°C.*

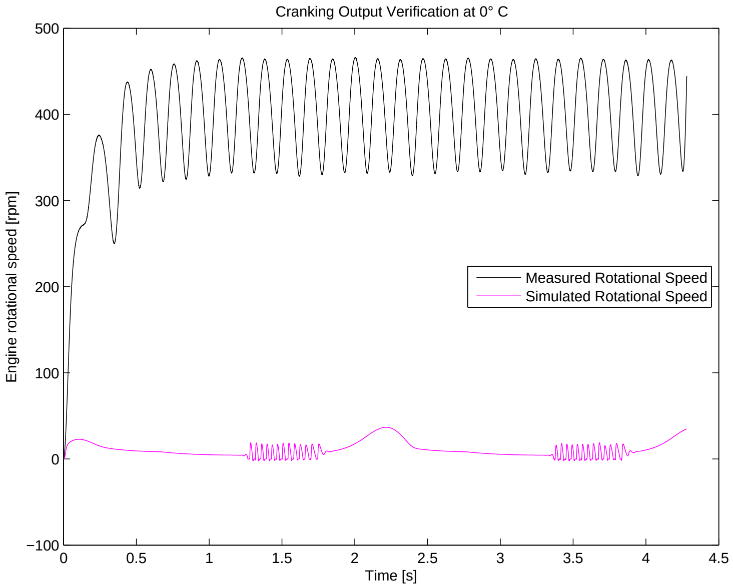

__Figure 4.19:__ Verification plot of Model 1 simulated at $0°C$.

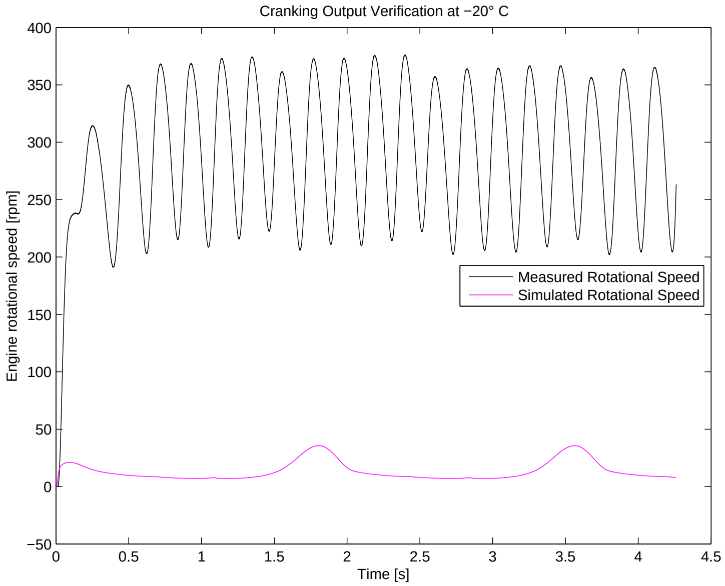

__Figure 4.20:__ Verification plot of Model 1 simulated at $-20°C$.

The high-frequency components present in the model outputs of Figures 4.18 and 4.19 originate in the friction submodel of the ICE model. As mentioned there are several parameters in this submodel that have been estimated with high uncertainty and the conclusion is that the high-frequency components stem from a badly calibrated engine friction model.

It is worth noting about the verification of Model 1 that during cranking simulation the cost of the prediction error minimization algorithm stabilises at quite a high level for both the verification simulations and the estimation cases, too high for the model to serve the purpose of this thesis. This means that the estimator is unable to bring the model output to a level matching the measured output, for any estimation data set. It appears that the current estimation approach of Model 1 is not able to duplicate the cranking scenario.

Figures 4.21 to 4.23 contain verification plots of Model 2 for the same scenarios as above for Model 1, three simulations at $+32°C$, $0°C$ and $-20°C$.

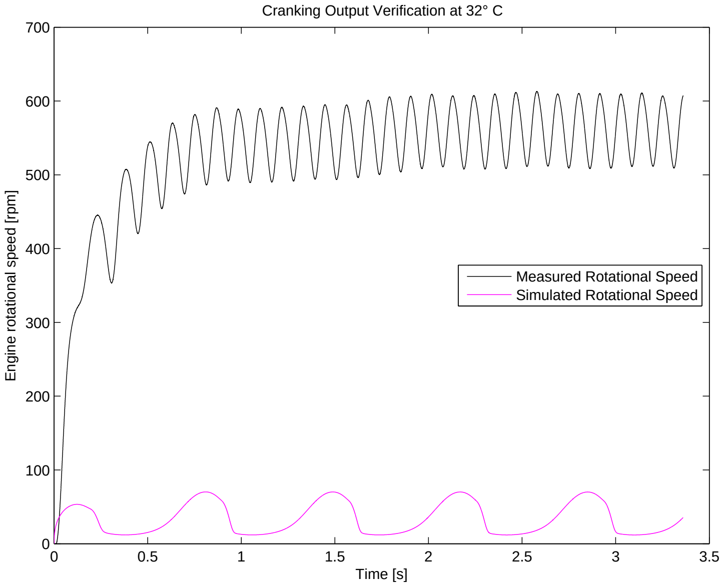

Figure 4.21: *Verification plot of Model 2 simulated at* $32°C$.

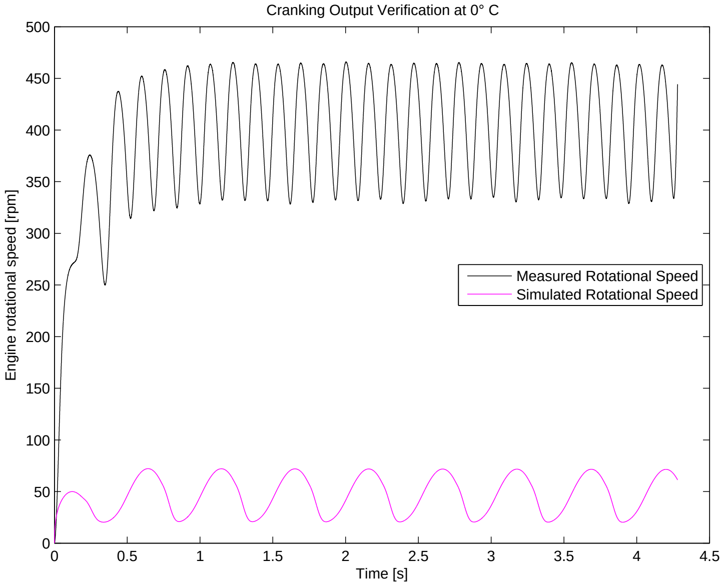

Figure 4.22: *Verification plot of Model 2 simulated at* $0°C$.

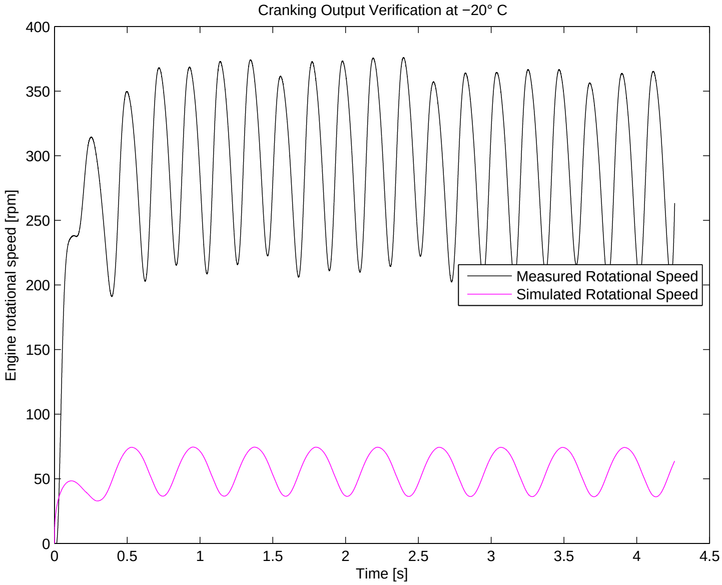

Figure 4.23: *Verification plot of Model 2 simulated at* $-20°C$.

It appears that the simulations of Model 2, represented in Figures 4.21 to 4.23, runs better than the the simulations of Model 1. The non-physical high-frequency elements of the output signal caused by the friction model in Model 1 are not present in the Model 2 simulations. This is a general property for the Model 2 simulations. Another difference is the higher base level of the rotational speed oscilations of the Model 2 outputs in Figures 4.21 to 4.23. The Model 1 simulated outputs tend to reach zero and at times even oscillate below this level. The Model 2 outputs oscillate in a manner more similar to the measured outputs, but with the wrong frequency, amplitude and base oscillation level.

While both Model 1 and Model 2 fail to model the desired outputs, Model 2 does appear to be a generally better model, confirming that the improvements made from Model 1 to Model 2 are relevant. It is worth noting that the simulation times for the verifications of Model 2 are significantly lower than the corresponding times for Model 1. Execution and estimation time of the models has proved an important factor in the thesis work, making the smoother running of Model 2 a significant advantage for it.

5

Conclusions

A battery model of the battery during cranking discharge has been implemented and included in the two cranking models. In the model evaluation, the battery model is able to model the fast dynamics of the voltage signals. There is a drift effect, seen in Figures 4.5, 4.6 and 4.8, that the model struggles to represent. This could be due to inaccurate SOC data or a model error. If there is a model error it is likely originating in the battery EMF model or the battery SOC model.

The different models of the electric machine and the engine are developed and compared: The electrical model parameters are estimated with similar accuracy as in Model 1, see Figures 4.14 and 4.17. The non-physical high-frequency components present in the simulations of Model 1 are not present in the simulations of Model 2. The electric motor rotational speed, ω_{em}, is known in relation to ω_e and therefore its addition to Model 2 does not significantly increase model complexity. Model 2 also models the rotational speed signal with varying amplitude, frequency and base level of oscillations during cranking, though they currently do not fit the measured signal. Estimation and simulation times are significantly lower for Model 2 compared to Model 1, and the added estimation signal, I, used for Model 1 does not aid accuracy in Model 1. In summary, Model 2 is the preferred cranking model for the purpose of this thesis.

With respect to the objectives of the thesis in Chapter 1 the components of the cranking system of a heavy duty truck engine have been identified. The causality and structure of a physical state-space model have been presented. The model has been implemented in *MATLAB/Simulink* in such a way that the models can be fitted to measurement data. The models have been fitted and their accuracy evaluated. While the cranking models are not at this stage able to accurately model the desired process there are no reasons in this thesis to dismiss the approach taken. Physical state-space modelling could be a viable way to implement a model for model-based condition estimation of heavy duty truck batteries, though further efforts are needed. Two directions for possible future work on the project have been given, see Section 5.1.

5.1 Future Work

There are two primary directions for future work on the modelling done in this thesis; to improve the model estimation and to improve the model structure.

To improve the model estimation involves investigating different estimation algorithms and softwares. In this case the problem is to be viewed as a non-linear model estimation problem. The implementation of the model is currently done in *MATLAB/Simulink* as this was a prerequisite of the thesis. Alternating the implementation of the current model structure would also be a course of action when attempting to improve model estimation.

The second course of action for future work would involve to improve or change the current model structure, i.e. the model equations, states and parameters. The friction model currently implemented in the ICE submodel uses model parameters that are generally estimated with large variance, see Figures 4.11 to 4.13 and Figures 4.15 to 4.17. The friction model also includes the highest number of model parameters of any submodel. An overview of this model and the manner in which its model parameters are obtained would be advisable.

As mentioned above in this chapter, the battery model is currently unable to correctly capture all tendencies of the measured battery. It would be advisable to review the model structure of this model in addition to the friction model when attempting to improve the overall model.

Bibliography

[1] Starting system general layout, September 2014. URL `http://lh5.ggpht.com/_IilukGkfijY/SqnywCw7SvI/AAAAAAAACno/YKaE06B6Q9Y/s1600-h/clip_image0063.jpg`. Cited on page 6.

[2] Operation of a dc motor 1, September 2014. URL `https://web.dsbn.edu.on.ca/~credit.recovery/SPH/SPH4CPU04/SPH4CPU04A06/images/image17.png`. Cited on page 10.

[3] Stribeck curve, September 2014. URL `http://www.stle.org/images/dev/image7.jpg`. Cited on page 13.

[4] Scania AB. Motorer, September 2014. URL `http://www.scania.se/lastbilar/main-components/engines/`. Cited on page 11.

[5] Charles Kingsley Jr. A.E. Fitzgerald and Stephen D. Umans. *Electric Machinery*. McGraw-Hill, 6th edition, 2003. Cited on pages 10, 23, and 24.

[6] Margaret A. Casacca and Ziyad M. Salameh. Determination of Lead-Acid Battery Capacity via Mathematical Modeling Techniques. *IEEE Transactions on Energy Conversions*, 7(3), September 1992. Cited on page 9.

[7] A.P. Koutroubousis C.D. Rakopoulos, D.T. Hountalas and T.C. Zannis. Application and Evaluation of a Detailed Friction Model on a DI Diesel Engine with Extremely High Peak Combustion Pressures. Technical report, SAE International, 2002. Cited on pages 12, 13, and 18.

[8] H.L. Chan and D. Sutanto. A New Battery Model for use with Battery Energy Storage Systems and Electric Vehicle Power Systems. *Power Engineering Society Winter Meeting, IEEE*, 2000. Cited on page 9.

[9] Naeim Henein Dinu Taraza and Walter Bryzik. Friction Losses in Multi-Cylinder Diesel Engines. Technical report, SAE International, 2000. Cited on page 13.

[10] Lars Eriksson and Ingemar Andersson. An Analytic Model for Cylinder Pressure in a Four Stroke SI Engine. Technical report, SAE International, 2002. Cited on pages 26 and 27.

[11] Lars Eriksson and Lars Nielsen. *Modeling and Control of Engines and Drivelines*. John Wiley and Sons, 1st edition, 2014. Cited on pages 11, 12, 14, 25, 26, 27, and 30.

[12] Daniel Gerhardsson. Starter Motor Protection. Master's thesis, Linköping University, SE-581 83 Linköping, 2010. Cited on pages 10, 11, 23, 24, 25, and 32.

[13] Shen Guo. The Application of Gentic Algorithms to Parameter Estimation in Lead-Acid Battery Equivalent Circuit Models. Master's thesis, University of Birmingham, 2010. Cited on pages 7, 8, and 19.

[14] Lino Guzzella and Antonio Sciarretta. *Vehicle Propulsion Systems*. Springer-Verlag Berlin Heidelberg, 3rd edition, 2013. Cited on pages 7, 9, 10, 11, 18, 19, 23, and 37.

[15] Haade. Serie shunt compound, February 2012. URL `http://commons.wikimedia.org/wiki/File:Serie_Shunt_Coumpound.svg?uselang=sv`. Cited on page 11.

[16] Robert A. Jackey. A Simple, Effective Lead-Acid Battery Modeling Process for Electrical System Component Selection. Technical report, The Mathworks Inc., 2007. Cited on pages 19, 20, 21, and 37.

[17] David Linden and Thomas B. Reddy. *Linden's Handbook of Batteries*. McGraw-Hill, 4th edition, 2011. Cited on pages 7, 19, and 20.

[18] Georgios Livanos. Development of a Simplified Instantaneous Friction Model of the Piston-Crank-Slider Mechanism of Internal Combustion Engines. *SAE Internatinal Journal of Engines*, 4:581–596, 2011. Cited on page 18.

[19] Lennart Ljung. Prediction error estimation methods. Technical Report LiTH-ISY-R-2365, Department of Electrical Engineering, Linköping University, October 2001. Cited on page 36.

[20] Lennart Ljung and Torkel Glad. *Modellbygge och Simulering*. Studentlitteratur, 2004. Cited on pages 18, 32, 37, and 40.

[21] Inc. Mathworks. System identification toolbox documentation, October 2014. URL `http://www.mathworks.se/help/ident/`. Cited on pages 35 and 36.

[22] Fredrik Mellblom. Start modelling for heavy trucks. Master's thesis, Linköpings Universitet, SE-581 83 Linköping, 2004. Cited on page 24.

[23] Mattias Millinger. Startprestanda. Technical Report 7003039, Scania AB, September 2008. Cited on page 36.

[24] Nazih Moubayed, Janine Kouta, Ali El-Ali, Hala Demayka, and Rachid Outbib. Parameter Identification of the Lead-Acid Battery Model. Technical report, Faculty of Engineering 1 at The Lebanese University and Laboratory of Sciences in Information and Systems at Aix-Marseille III University, 2008. Cited on pages 19 and 37.

[25] Ahmad A. Pesaran. Battery Thermal Models for Hybrid Vehicle Simulations. *Journal of Power Sources*, 110, 2002. Cited on page 7.

[26] Sohair F. Rezeka and Naeim A. Henein. A New Approach to Evaluate Instantaneous Friction and Its components in Internal Combustion Engines. Technical report, SAE International, 1984. Cited on pages 12, 18, and 28.

[27] Daniel Sandoval. An Improved Friction Model for Spark Ignition Engines. Bachelor's Thesis, Department of Mechanical Engineering, Massachusetts Institute of Technology, May 2002. Cited on pages 12, 18, and 28.

[28] Chrisopher Souzzo. Lead-Acid Battery Aging and State of Health Diagnosis. Master's thesis, The Ohio State University, 2008. Cited on pages 7, 8, 9, 19, and 22.

[29] Y.H. Zweiri, J.F. Whidborne, and L.D. Seneviratne. Instantaneous Friction Components Model for Transient Engine Operation. *Journal of Automobile Engineering*, 2000. Cited on pages 12, 13, 14, 18, 28, 29, 30, and 31.

Linköpings universitet

Upphovsrätt

Detta dokument hålls tillgängligt på Internet — eller dess framtida ersättare — under 25 år från publiceringsdatum under förutsättning att inga extraordinära omständigheter uppstår.

Tillgång till dokumentet innebär tillstånd för var och en att läsa, ladda ner, skriva ut enstaka kopior för enskilt bruk och att använda det oförändrat för icke-kommersiell forskning och för undervisning. Överföring av upphovsrätten vid en senare tidpunkt kan inte upphäva detta tillstånd. All annan användning av dokumentet kräver upphovsmannens medgivande. För att garantera äktheten, säkerheten och tillgängligheten finns det lösningar av teknisk och administrativ art.

Upphovsmannens ideella rätt innefattar rätt att bli nämnd som upphovsman i den omfattning som god sed kräver vid användning av dokumentet på ovan beskrivna sätt samt skydd mot att dokumentet ändras eller presenteras i sådan form eller i sådant sammanhang som är kränkande för upphovsmannens litterära eller konstnärliga anseende eller egenart.

För ytterligare information om Linköping University Electronic Press se förlagets hemsida `http://www.ep.liu.se/`

Copyright

The publishers will keep this document online on the Internet — or its possible replacement — for a period of 25 years from the date of publication barring exceptional circumstances.

The online availability of the document implies a permanent permission for anyone to read, to download, to print out single copies for his/her own use and to use it unchanged for any non-commercial research and educational purpose. Subsequent transfers of copyright cannot revoke this permission. All other uses of the document are conditional on the consent of the copyright owner. The publisher has taken technical and administrative measures to assure authenticity, security and accessibility.

According to intellectual property law the author has the right to be mentioned when his/her work is accessed as described above and to be protected against infringement.

For additional information about the Linköping University Electronic Press and its procedures for publication and for assurance of document integrity, please refer to its www home page: `http://www.ep.liu.se/`

© Erik Andersson